Supporting Information

Synthesis, Characterisation and Biological profiling of Ru(II) based 4-nitro- and 4-amino-1,8-naphthalimide conjugates

Robert B. P. Elmes,[a,h]* Gary J. Ryan,[b] MariaLuisa Erby,[c] Daniel O. Frimannsson,[b,] Jonathan A. Kitchen,[b,e] Mark Lawler,[f,g] D. Clive Williams,[c] Susan J. Quinn,[d,h]* and Thorfinnur Gunnlaugsson[b,h]*

[a] Department of Chemistry, Maynooth University, National University of Ireland, Maynooth, Co. Kildare, Ireland.

E-mail: robert.elmes@mu.ie; Tel: +353 1708 4615

[b]School of Chemistry, Trinity Biomedical Sciences Institute (TBSI), Trinity College Dublin, The University of Dublin, Dublin 2, Ireland

E-mail: gunnlaut@tcd.ie; Tel: +353 896 3459

[c] School of Biochemistry and Immunology, Trinity Biomedical Sciences Institute (TBSI), Trinity College Dublin, The University of Dublin, Dublin 2, Ireland

[d]School of Chemistry, University College Dublin, Dublin 4, Ireland

E-mail: susan.quinn@ucd.ie; Tel: +353 7162407

[e]Chemistry, School of Natural and Computational Sciences, Massey University, Auckland, New Zealand

[f]School of Medicine, Institute of Molecular Medicine, St. James's Hospital, Trinity College Dublin, Dublin 8, Ireland

[g]Institute for Health Sciences, Centre for Cancer Research and Cell Biology, School of Medicine, Dentistry and Biomedical Sciences, Queen's Univeristy of Belfst, Belfast BT9 7BL, Northern Ireland.

[h]Synthesis and Solid State Pharmaceutical Centre (SSPC), Ireland

General Experimental Techniques

All NMR spectra were recorded using either a 400 MHz Bruker Spectrospin DPX-400 or AV-600 spectrometer, operating at 400.1/600.1 MHz for ^{1}H NMR and 100.2/150.2 MHz for ^{13}C NMR respectively. Shifts are referenced relative to the internal solvent signals. Electrospray mass spectra were recorded on a Micromass LCT spectrometer or a MALDI QToF Premier, running Mass Lynx NT V 3.4 on a Waters 600 controller connected to a 996 photodiode array detector with HPLC-grade methanol or acetonitrile. High resolution mass spectra were determined by a peak matching method, using leucine enkephaline, (Tyr-Gly-Gly-Phe-Leu), as the standard reference (*m/z* = 556.2771). All accurate masses were reported within ±5 ppm. Melting points were determined using an IA9000 digital melting point apparatus. Infrared spectra were recorded on a Perkin Elmer Spectrum One FT-IR spectrometer fitted with a Universal ATR Sampling Accessory. Elemental analysis was conducted at the Microanalytical Laboratory, School of Chemistry and Chemical Biology, University College Dublin.

UV-visible absorption spectra were recorded on a Varian CARY 50 spectrophotometer with a wavelength range of 200-800 nm and a scan rate of 600 nm min^{-1}. Baseline correction measurements were used for all spectra. Fluorescence measurements were made with a Varian Carey Eclipse Fluorimeter in either 1 cm or 3 cm quartz cuvettes. The luminescence quantum yields were calculated relative to the reference value of $[Ru(bpy)_3]^{2+}$ (0.028 in H_2O). The quantum yields were determined from the integration of fluorescence spectra obtained in the reference solvent. The spectra were obtained under the same conditions using a solution of the same absorbance and excited at the same wavelength. Fluorescence lifetime experiments were carried out on a Horiba Scientific FluoroLog - Modular Spectrofluorometer equipped with Time Correlated Single Photon Counting (TCSPC) capability. Linear and Circular Dichroism (CD) spectra were recorded at a concentration corresponding to an optical density of approximately 1.0, in buffered solutions, on a J-815 Circular Dichroism Spectropolarimeter equipped with a Linear Dichroism Accessory (LD) or a Jasco J-810-150S CD spectropolarimeter (CD). Thermal denaturation experiments were performed on a thermoelectrically coupled Perkin Elmer LAMBDA 25 UV/Vis Spectrophotometer. The temperature in the cell was ramped from 30 to 90 ºC, at a rate of 1 ºC min^{-1} and the absorbance at 260 nm was measured every 0.2 ºC. All other reagents and solvents were purchased commercially and used without further purification. Solutions of DNA in 10mM phosphate buffer (pH 7.4) gave a ratio of UV absorbance at 260 nm and 280 nm of 1.86:1, indicating that the DNA was sufficiently free of protein. Its concentration was determined

spectrophotometrically using the molar absorptivity of 6600 M^{-1} cm^{-1} (260 nm). The concentration of homopolymers, $[poly(dAdT)]_2$ and $[poly(dGdC)]_2$ was also determined spectrophotometrically using the molar absortivities of 6600 M^{-1} cm^{-1} (262nm) and 8400 M^{-1} cm^{-1} (254nm), respectively. Phosphate buffer was made from two 1M stock solutions of NaH_2PO_4 and Na_2HPO_4 (using 10 mL volumetric flasks) in millipore water. Portions of each solution were diluted together to achieve 10 mM phosphate buffer and the pH was adjusted to pH 7.4 by addition of NaOH. Titrations were carried out on samples of the complexes at 1 (± 0.5) × 10^{-5} M at ambient temperature by monitoring changes in the absorption and emission spectra, at pH 7.4 in 10 mM phosphate buffer upon successive additions of aliquots of stDNA. The results are quoted using the concentration of stDNA expressed as a nucleotide phosphate to dye ratio (P/D ratio).

Calculation of binding constants from UV/Vis Titration Data

The intrinsic binding constant $\boldsymbol{K_b}$, and binding site size $\boldsymbol{n}$ were determined using the model of Bard *et al*.,[1] equation **(1)** from a plot of $\boldsymbol{(\varepsilon a-\varepsilon f)/(\varepsilon b-\varepsilon f)}$ vs. $\boldsymbol{[DNA]}$. $\boldsymbol{\varepsilon a}$, $\boldsymbol{\varepsilon f}$, $\boldsymbol{\varepsilon b}$ correspond to the apparent extinction coefficient, the extinction coefficient for the free dye, and the extinction coefficient for the dye in the fully bound form. $\boldsymbol{C_t}$ is the total dye concentration, $\boldsymbol{[DNA]}$ is the DNA concentration expressed in nucleotide phosphate. The data was fit to this model using non-linear regression with Sigmaplot 11.0.

$$\frac{(\boldsymbol{\varepsilon_a - \varepsilon_f})}{(\boldsymbol{\varepsilon_b - \varepsilon_f})} = \frac{[\boldsymbol{b} - (\boldsymbol{b^2} - \boldsymbol{2K_b + C_t[DNA]/n})^{\boldsymbol{1/2}}]}{(\boldsymbol{2K_bC_t})} \qquad \textbf{(1)}$$

$$\boldsymbol{b = 1 + K_b C_t + K_b[DNA]/2} \qquad \textbf{(2)}$$

General Biological Procedures

The DNA photocleavage studies were carried out by treating pBR322 plasmid DNA (1 mg/mL) with each of the complexes at varying ratios. The samples were then subjected to 2 J/cm^2 (30 mins irradiation) using an Hamamatsu L2570 200 Watt HgXe Arc Lamp equipped with a $NaNO_2$ filter before being separated using horizontal agarose gel electrophoresis in a TBE (90 mM Tris-borate, 2 mM EDTA, pH 8.0) buffer. A 0.8% (*w/v*) agarose solution was prepared by dissolving 0.8 g of agarose in 100 mL of TBE buffer. The agarose was melted by boiling, and the gel was poured while warm and left to cool. Electrophoresis was carried out at *ca.* 5 V/cm

(40 mA, 90 V) to separate covalently closed circular (**Form I**), open circular (**Form II**), and linear (**Form III**) forms of the plasmid DNA. A loading dye solution composed of sucrose (40%), xylene-cyanol (0.25%), and bromophenol (0.25%) in TBE was added to the samples to help them sink in the wells of the gel. DNA migrated less rapidly than the xylene-cyano1 dye (green), with bromophenol blue (violet) moving more rapidly. Visualisation of the DNA after electrophoresis was achieved by staining the gel for 90 mins with an aqueous solution of ethidium bromide, which fluoresces strongly when bound to DNA. The dye within the gel was illuminated with a transilluminator (Bioblock 254 UV illuminator) and the gel photographed to provide a record of the distances migrated by the various DNA fragments. The ratio of the different forms was estimated using ImageJ Gel analysis software.

HeLa cells were grown in a cell culture flask using low-glucose Dulbecco's Modified Eagle Medium supplemented with 10% fetal bovine serum at 37 °C in a humidified atmosphere of 5% CO_2. Confocal microscopy experiments were carried out using HeLa cells, seeded at a density of *ca.* 1×10^5 cells/2mL. Cells were left for the appropriate incubation time before treatment with the required complex for varying incubation times. Cells were washed twice with fresh media to remove excess compound before detection of fluorescence between 580 and 680 nm using an Olympus FV1000 point scanning microscope fitted with a 60x oil immersion lens with an NA (numerical aperture) of 1.42. The software used to collect images was FluoView Version 7.1 software.

Materials

All chemicals were obtained from Sigma-Aldrich, TCI or Alfa Aesar and unless specified, were used without further purification. Deuterated solvents for NMR use were purchased from Apollo Ltd. Dry solvents were prepared using standard procedures, according to Vogel's Textbook of Practical Organic Chemistry (5th Edition), with distillation prior to each use. Chromatographic columns were run using Silica gel 60 (230-400 mesh ASTM). Solvents for synthetic purposes were used at GPR grade unless otherwise stated. Analytical TLC was performed using Merck Kieselgel 60 F_{254} silica gel plates. *cis*-$[Ru(bpy)_2Cl_2]$,[2] *cis*-$[Ru(TAP)_2Cl_2]$[3] and $[RuCl_2(\eta^4\text{-COD})]$[4] were prepared by the literature routes. The stDNA, and homopolymers, $[poly(dA\text{-}dT)]_2$ and $[poly(dG\text{-}dC)]_2$, were obtained from Sigma Aldrich as their sodium salts and were stored at -20 ˚C.

X-ray Crystallography

X-ray data were collected on a Rigaku Saturn 724 CCD Diffractometer using graphite-monochromated Mo Ka radiation (k = 0.71073 Å). The datasets were collected using Crystal clear-SM 1.4.0 software. Data integration, reduction and correction for absorption and polarization effects were all performed using Crystalclear-SM 1.4.0 software. Space group determinations were obtained using Crystal structure ver. 3.8. The structure was solved by direct methods using SHELXS-2017 [5] and refined on F_O^2 using Olex2.refine.[6] H-atoms were positioned geometrically and refined using a riding model. The solvent mask routine in Olex2 was required to remove the contribution from a severely disordered PF_6^- counter ion in **6** that could not be modelled despite many attempts. The total accessible volume per unit cell was 483.4 Å^3 and total electron count per unit cell was 164. This corresponded very well to one PF_6^- molecule (expected electron count of 70) and one water molecule (expected electron count of 10 per complex) per complex, giving 160 electrons per unit cell. The removed PF_6^- appeared to be disordered over multiple sites and during attempts to model the disorder, two partial (~0.5) occupancy octahedral PF_6^- molecules could be found, however despite using a range of restraints (e.g. DFIX, SADI, SAME, DANG) the refinement was not stable. Instead the use of the smbt-solvent mask routine in Olex2 was used to account for the disordered PF_6^- and give a better refinement for the remainder of the molecule. The nature of the removed component is not in doubt, neither is the oxidation state of the metal centre (as determined by other characterisation techniques - NMR analysis, Mass Spectrometry). Refinement details for **6** can be found in the crystallographic information file (CCDC 2002583). **Crystal Data** for $C_{50}H_{37}F_6N_9O_2PRu$ (M =1041.94 g/mol): triclinic, space group P-1 (no. 2), a = 14.065(9) Å, b = 14.572(9) Å, c = 14.834(8) Å, α = 104.634(8)°, β = 107.989(8)°, γ = 95.848(3)°, V = 2744(3) Å^3, Z = 2, T = 117.15 K, μ(Mo Kα) = 0.379 mm^{-1}, $Dcalc$ = 1.2609 g/cm^3, 80600 reflections measured (4.68° ≤ 2Θ ≤ 49°), 9126 unique (R_{int} = 0.1044, R_{sigma} = 0.0737) which were used in all calculations. The final R_1 was 0.0957 (I>=2u(I)) and wR_2 was 0.2578 (all data).

Synthetic Procedures

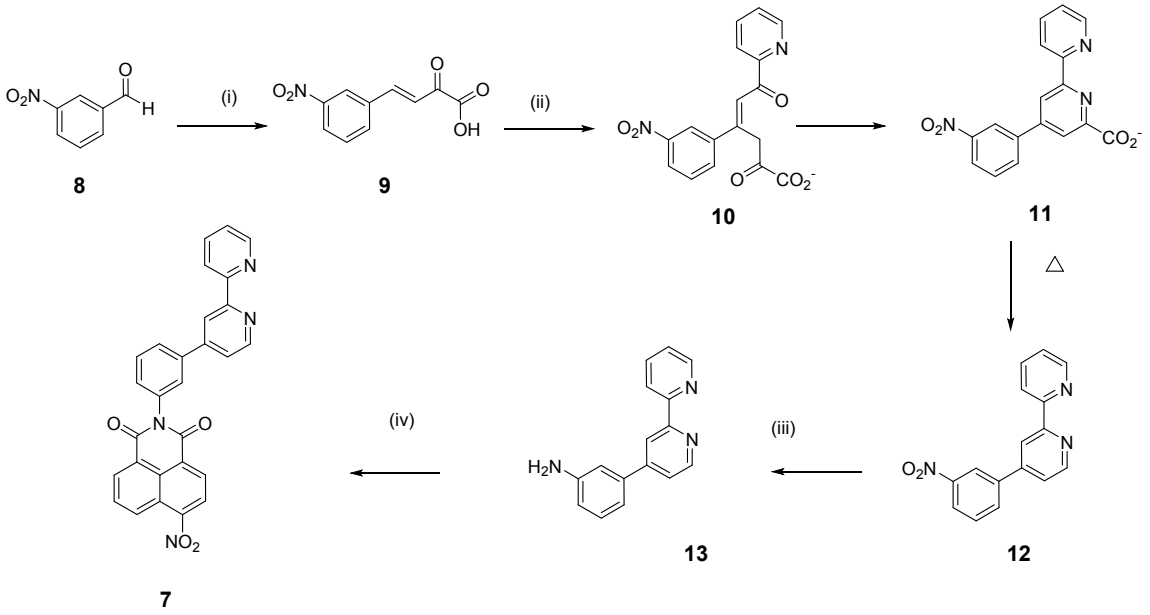

***Scheme S1**: **Synthesis of Ligand 7** (i) EtOH, sodium pyruvate, NaOH; (ii) ammonium acetate, H_2O; (iii) EtOH, N_2H_2, 10%Pd; (iv) EtOH, 4-nitro-naphthalic anhydride.*

General Conditions for Complexation with $Ru(L\text{-}L)_2Cl_2$

Ligand **7** (1 eq.) and the appropriate $Ru(L\text{-}L)_2Cl_2$ complex (1 eq.) were suspended in an either EtOH:H_2O or DMF:H_2O mixture (1:1, 7 mL) before the suspension was degassed by bubbling with argon for 15 mins. The mixture was heated at 140 °C for 40 mins using microwave irradiation and filtered before the PF_6 salt of the complex was precipitated from solution by addition of a conc. ethanolic solution of NH_4PF_6. The resultant precipitate was collected *via* centrifugation before being washed with H_2O (5 mL), EtOH (5 mL) and Et_2O (5 mL). Purification was achieved either through silica gel flash column chromatography eluting with CH_3CN/H_2O/Aq. $NaNO_{3(sat)}$ (40:4:1) or by ether diffusion into a concentrated sample in CH_3CN. The product was dried under vacuum before the chloride form of the complex was reformed by stirring a solution of the PF_6 complex in MeOH (15 mL) in Amberlite ion exchange resin (chloride form) for 1 hr.

4-(3-Nitrophenyl)-2-oxobut-3-enoic acid (9)

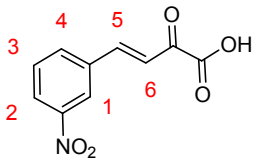

3-Nitro-benzaldehyde **8** (7.7 g, 51.1 mmol, 1 eq.) was added to EtOH and the mixture heated to 70 ºC until the solid dissolved. Sodium pyruvate (6.2 g, 56.2 mmol, 1.1 eq.) dissolved in H_2O was added, and the mixture cooled to 0 °C in an ice bath. NaOH solution (2M, 30 mL) was added dropwise and the mixture stirred at 0 °C for 3 hrs. The mixture was subsequently neutralised with 2M HCl, filtered, the solid washed with EtOH (2 × 10 mL) and

dried giving the product as a bright yellow solid (6.19 g, 54%). δ_H (400 MHz, [D_6] DMSO): 8.45 (s, 1H, H-1), 8.22 (dd, 1H, *J* = 2.0, *J* = 8.0, H-2), 8.15 (d, 1H, *J* = 8.0, H-4), 7.70 (t, 1H, *J* = 8.0, H-3), 7.54 (d, 1H, *J* = 16.6, H-5), 7.05 (d, 1H, *J* = 16.6, H-6). δ_C (100 MHz, [D_6] DMSO): 196.8, 169.2, 148.8, 141.3, 137.1, 134.5, 130.9, 127.9, 124.8, 123.0. ν_{max} (film)/cm^{-1}: 3502 (-O-H), 1688 (C=O), 1535 (C-NO_2), 1346 (C-NO_2). HRMS (*m/z* -ES): Found: 220.0252 (M-H. $C_{10}H_6NO_5$ Requires: 220.0246).

4-(3-Nitrophenyl)-2,2'-bipyridine (12)

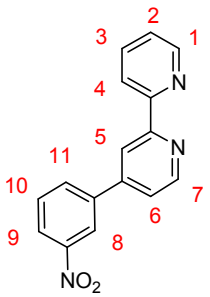

4-(3-nitrophenyl)-2-oxobut-3-enoic acid **9** (2.13 g, 9.63 mmol, 1 eq.), 2-pyridacyl pyridinium iodide (3.14 g, 9.63 mmol, 1 eq.) and ammonium acetate (5.95 g, 77.21 mmol, 8 eq.) were added to H_2O and the mixture heated at reflux for 5 hrs. The solid was filtered, and washed with H_2O (2 × 10 mL) and acetone (2 × 5 mL). The ammonium salt was heated under high vacuum with a heat gun until evolution of CO_2 ceased. The resulting black solid was dissolved in EtOAc (150 mL), activated charcoal added and the mixture refluxed for 15 mins. The mixture was filtered through a pad of celite and the solvent removed under reduced pressure to yield the product as a pale yellow solid (2.67 g, 51%). δ_H (400 MHz, $CDCl_3$): 8.80 (d, 1H, *J* = 4.8, H-7), 8.73 (m, 2H, H-5 and H-1), 8.62 (app d, 1H, H-8), 8.48 (d, 1H, *J* = 8.0, H-4), 8.31 (d, 1H, *J* = 8.0, H-9), 8.10 (d, 1H, *J* = 8.0, H-11), 7.86 (t, 1H, *J* = 8.0, H-3), 7.72 (t, 1H, *J* = 8.0, H-10), 7.58 (d, 1H, *J* = 5.0, H-6), 7.36 (t, 1H, *J* = 6.0, H-2). δ_C (100 MHz, $CDCl_3$): 157.4, 155.8, 150.2, 149.4, 149.1, 147.0, 140.4, 137.2, 133.3, 130.3, 124.3, 123.9, 122.3, 121.6, 121.5, 119.1. ν_{max} (film)/cm^{-1}: 1529 (C-NO_2), 1349 (C-NO_2). HRMS (*m/z* -ES): Found: 278.0923 (M+H. $C_{16}H_{12}N_3O_2$ Requires: 278.0930).

3-([2,2'-Bipyridin]-4-yl)aniline (13)

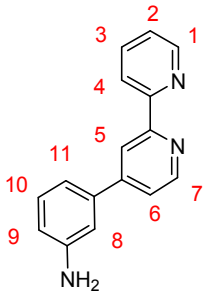

4-(3-Nitrophenyl)-2,2'-bipyridine **12** (0.87 g, 3.14 mmol, 1 eq.) and 10% Pd/C (0.2 g) were added to EtOH (30 mL) and the mixture heated at reflux for 1 hr. Hydrazine monohydrate (98%, 20 eq.) was added and the mixture heated at reflux for 1 hr. The mixture was filtered through a pad of celite and the solid washed with CH_2Cl_2 (40 mL). The filtrate was washed with water, dried over $MgSO_4$, and the solvent removed under reduced pressure yielding the product as an off white solid (0.73 g, 94%). δ_H (400 MHz, $CDCl_3$): 8.75 (m, 2H, H-1 and H-7), 8.65 (d, 1H, *J* = 1.2, H-5), 8.47 (d, 1H, *J* = 7.8, H-4), 7.86 (dt, 1H, *J* = 7.8, *J* = 1.5, H-3), 7.53 (dd, 1H, *J* = 5.0, *J* = 1.76, H-6), 7.33 (m, 2H, H-2 and H-

10), 7.17 (d, 1H, *J* = 7.8, H-11), 7.11 (s, 1H, H-8), 6.79 (dd, 1H, *J* = 7.8, *J* = 1.6, H-9), 3.85 (s, 1H, NH_2). δ_C (100 MHz, $CDCl_3$): 156.5, 156.2, 149.6, 149.2, 147.0, 139.4, 137.0, 130.0, 123.8, 121.7, 121.3, 119.0, 117.5, 115.7, 113.6. ν_{max} (film)/cm^{-1}: 3429 (NH_2 Stretch), 1632 (Aromatic C-N). HRMS (*m/z* -ES): Found: 248.1198 (M+H. $C_{16}H_{14}N_3$ Requires: 248.1188).

4-[*N*-phenyl-4-nitro-1,8-napthalimide]-2,2'-bipyridine (7)

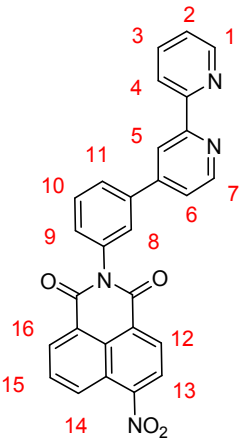

3-([2,2'-bipyridin]-4-yl)aniline **13** (0.54 g, 2.17 mmol, 1 eq.) and 4-nitro-1,8-naphthalic anhydride (0.53 g, 2.17 mmol, 1 eq.) were suspended in HPLC grade EtOH (30 mL) and the mixture refluxed in a pressure tube for 48 hrs. The reaction mixture was cooled to room temperature before the product was collected by suction filtration and washed with EtOH (30 mL) giving the product as a yellow/brown solid (0.86 mg, 84%). δ_H (400 MHz, $CDCl_3$): 8.92 (d, 1H, *J* = 8.7, H-14), 8.81 (d, 1H, *J* = 7.4, H-16), 8.75 (m, 2H, H-7 and H-13), 8.7 (s, 1H, H-5), 8.68 (d, 1H, *J* = 5.0, H-1), 8.46 (m, 2H, H-4 and H-12), 8.05 (t, 1H, *J* = 7.8, H-15), 7.93 (d, 1H, *J* = 8.0, H-9), 7.84 (t, 1H, *J* = 8.0, H-3), 7.72 (m, 2H, H-8 and H-10), 7.59 (d, 1H, *J* = 5.0, H-6), 7.42 (d, 1H, *J* = 7.5, H-11), 7.32 (t, 1H, *J* = 6.0, H-2).δ_C (100 MHz, $CDCl_3$): 162.2, 156.3, 155.5, 149.5, 149.3, 148.7, 147.7, 139.5, 136.5, 135.0, 132.5, 129.9, 129.8, 129.7, 129.4, 129.0, 128.6, 127.4, 126.9, 126.5, 123.6, 123.5, 123.4, 122.6, 121.2, 120.9, 118.6. ν_{max} (film)/cm^{-1}: 1717 (-CO-N-CO-), 1524 (C-NO_2), 1350 (C-NO_2). HRMS (*m/z* -ES): Found: 473.1233 (M+H. $C_{28}H_{17}N_4O_4$ Requires: 473.1250).

NMR Characterisation:

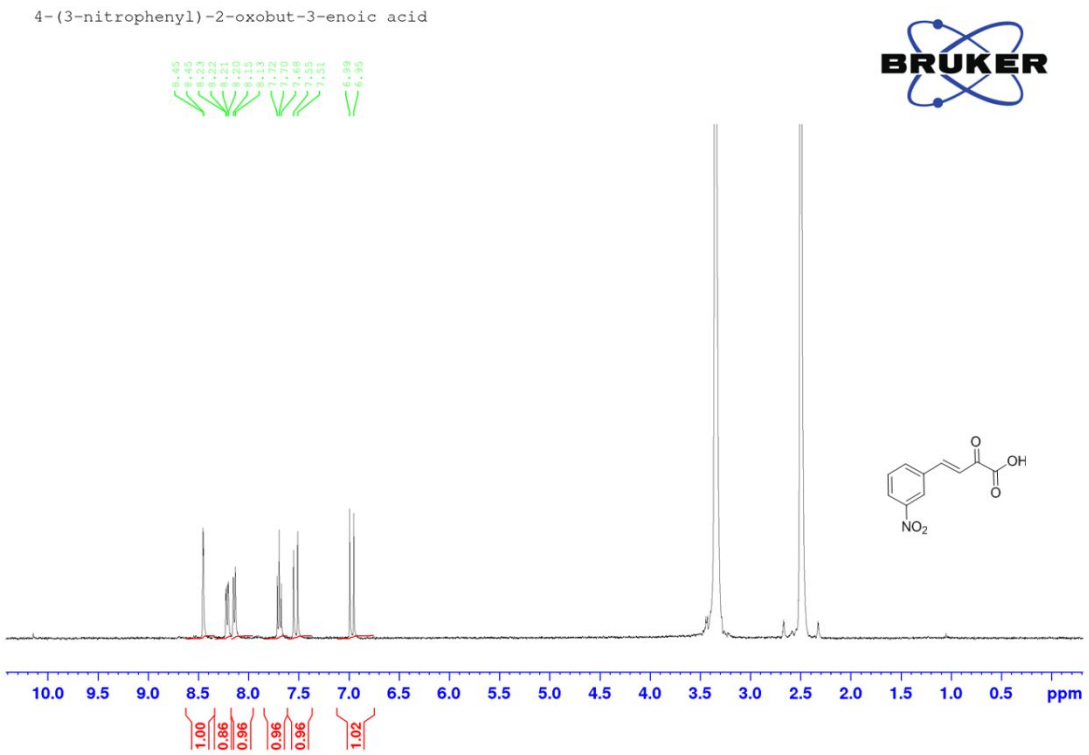

Figure S1: ^{1}H NMR (DMSO-d_6, 500 MHz) spectrum of **9**.

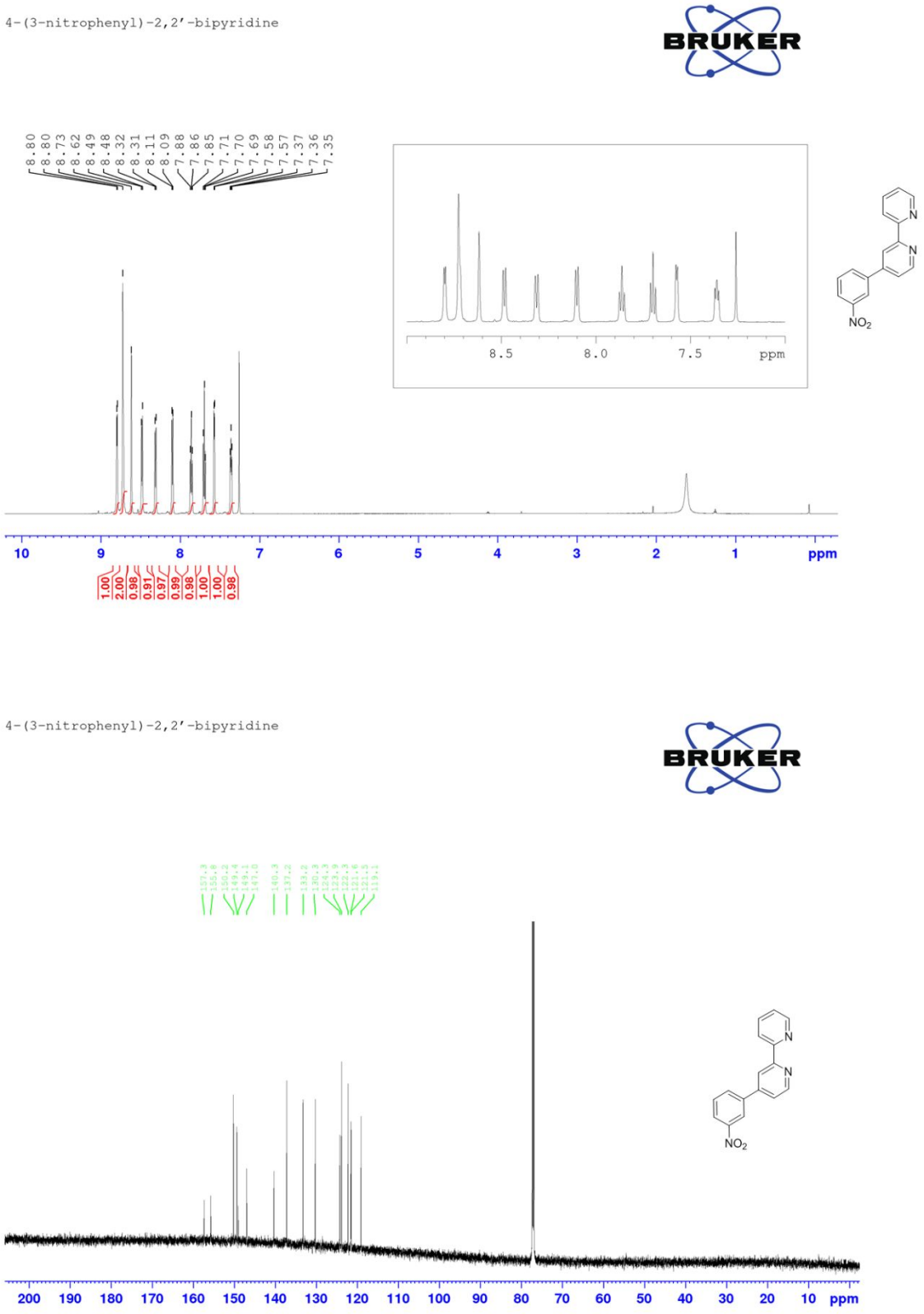

Figure S2: ^{1}H NMR ($CDCl_3$, 500 MHz) and ^{13}C NMR ($CDCl_3$, 125 MHz) spectra of **12**.

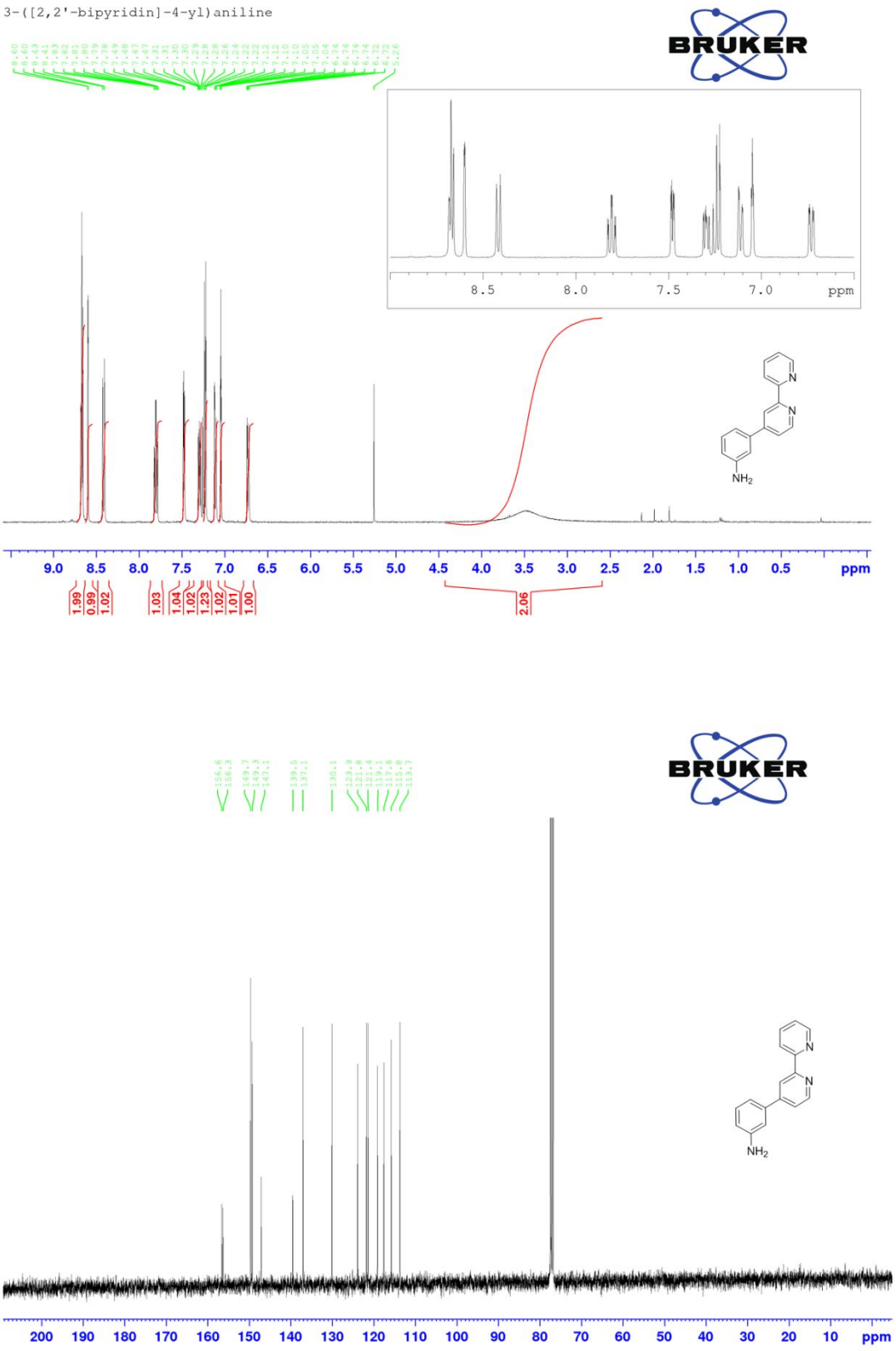

Figure S3: ^{1}H NMR ($CDCl_3$, 500 MHz) and ^{13}C NMR ($CDCl_3$, 125 MHz) spectra of **13**.

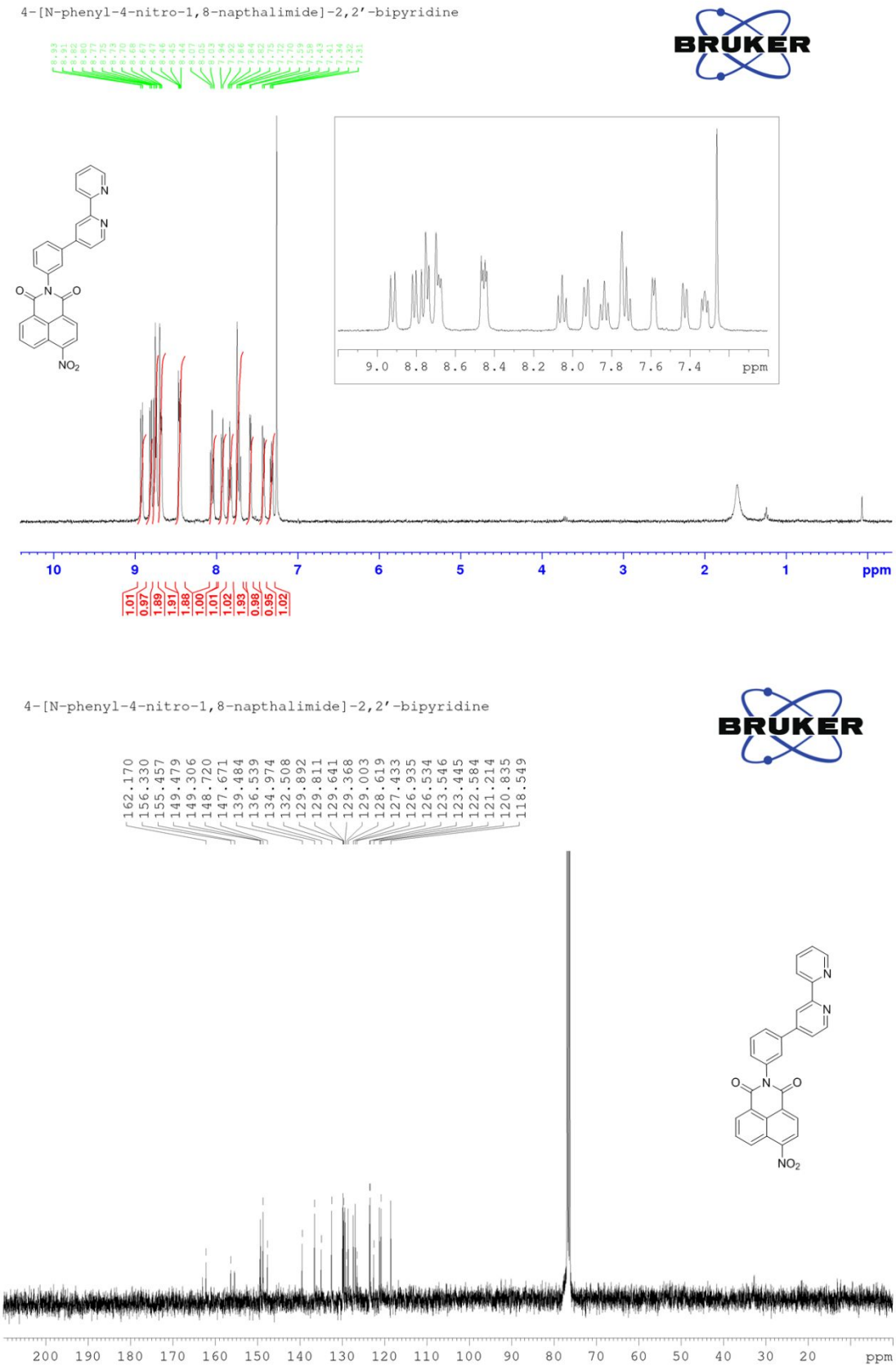

Figure S4: ^{1}H NMR ($CDCl_3$, 500 MHz) and ^{13}C NMR ($CDCl_3$, 125 MHz) spectra of **7**.

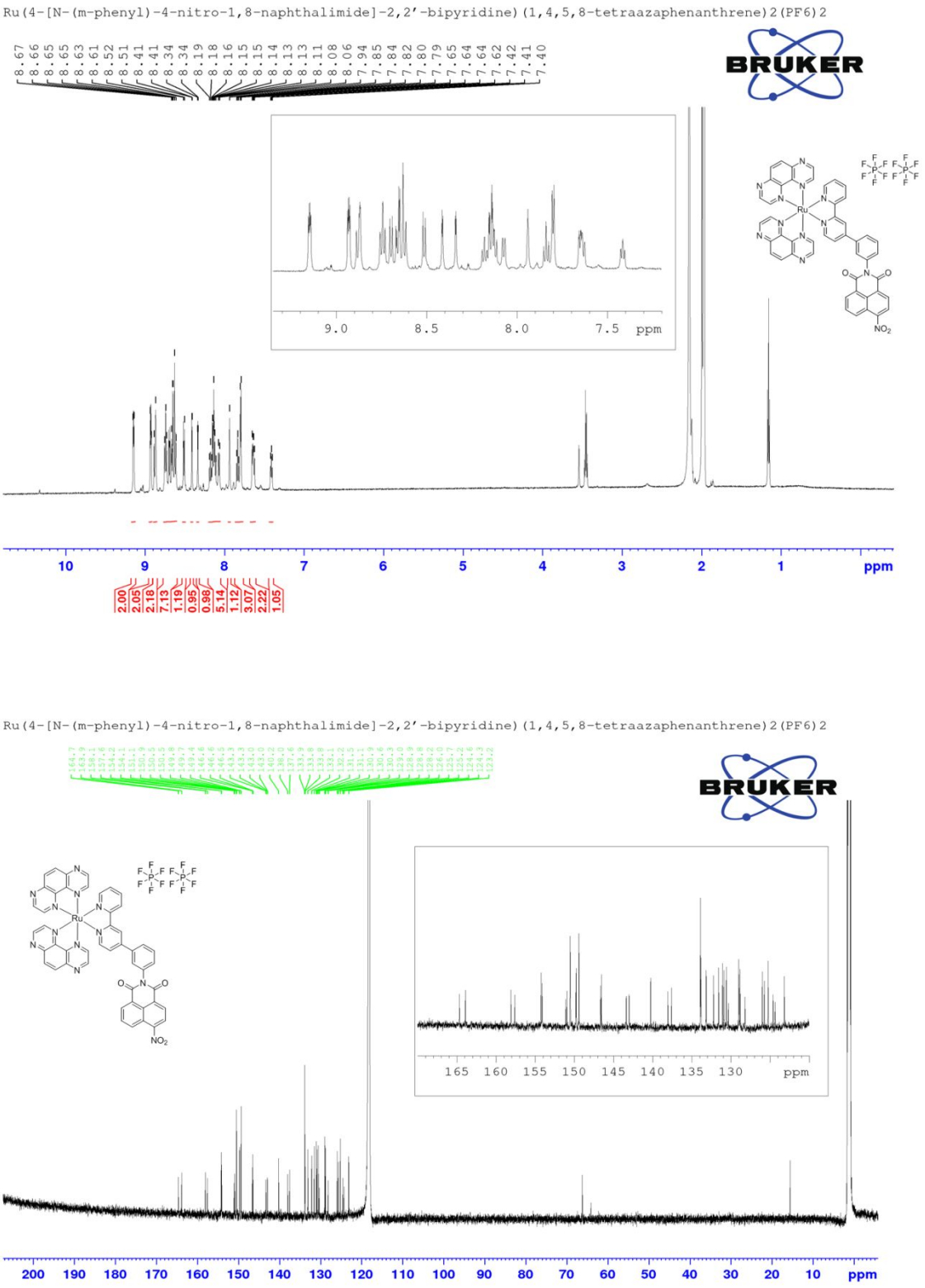

Figure S5: ^{1}H NMR (CD_3CN, 500 MHz) and ^{13}C NMR (CD_3CN, 125 MHz) spectra of **1**.

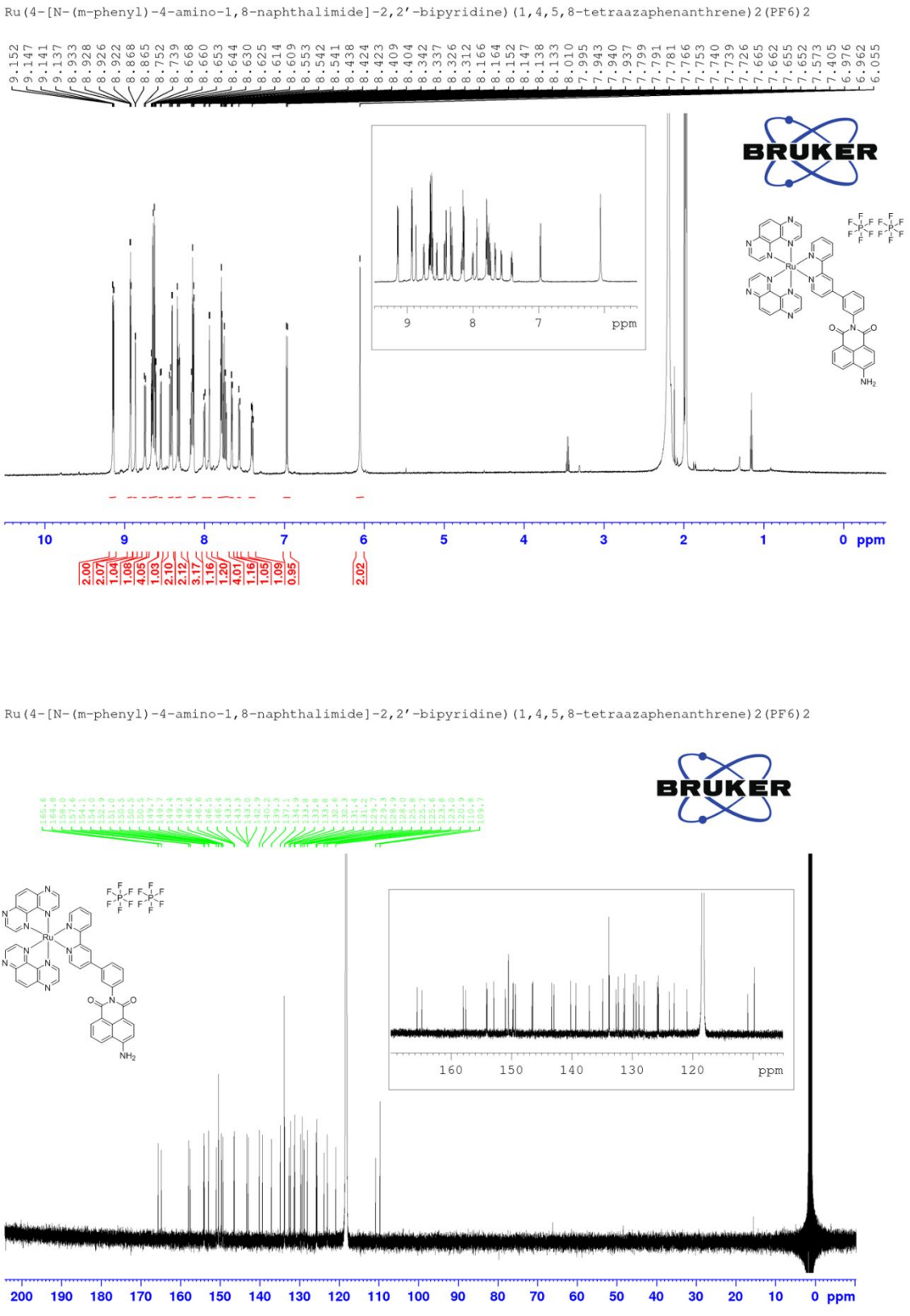

Figure S6: ^{1}H NMR (CD_3CN, 500 MHz) and ^{13}C NMR (CD_3CN, 125 MHz) spectra of **2**.

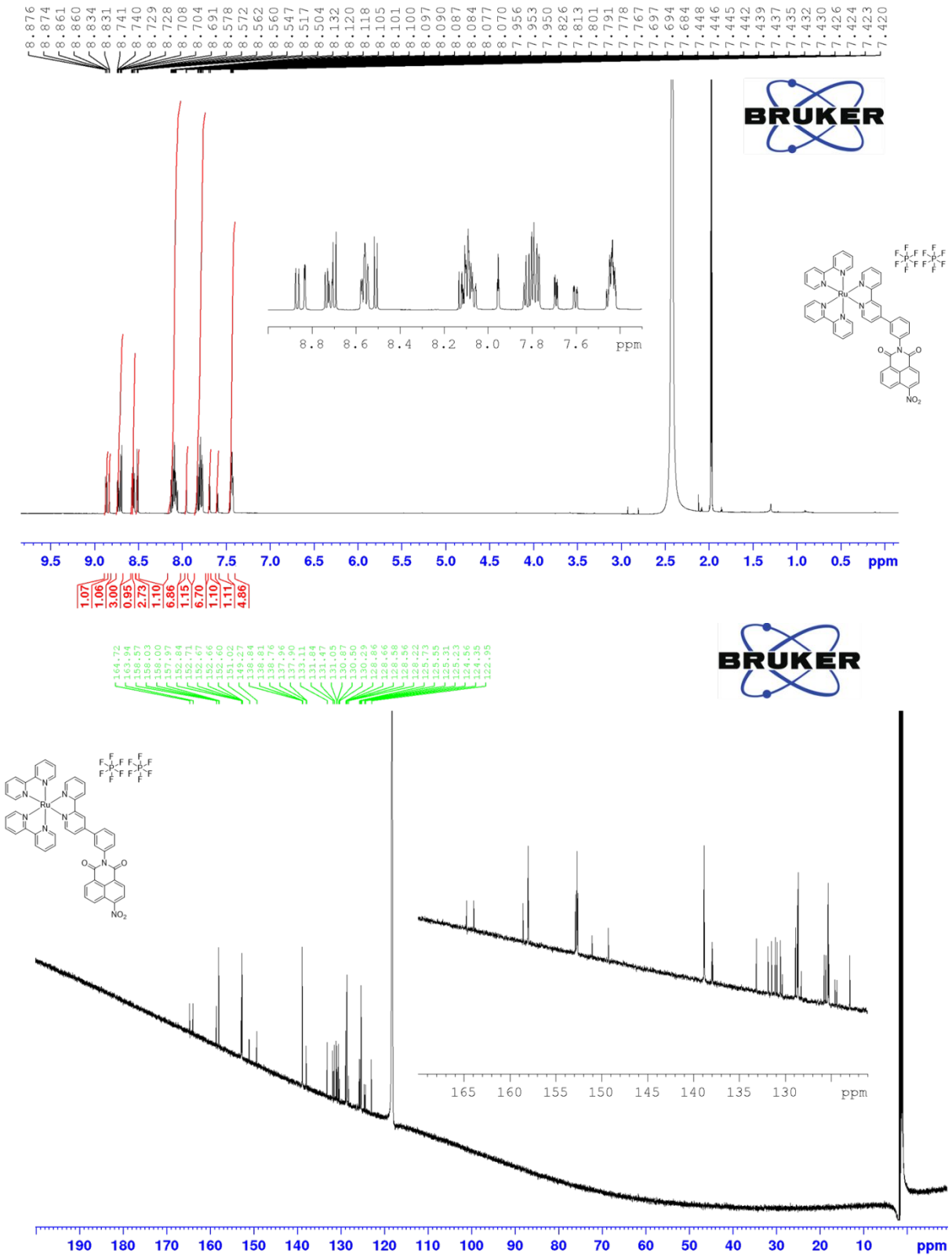

Figure S7: ^{1}H NMR (CD_3CN, 500 MHz) and ^{13}C NMR (CD_3CN, 125 MHz) spectra of **3**.

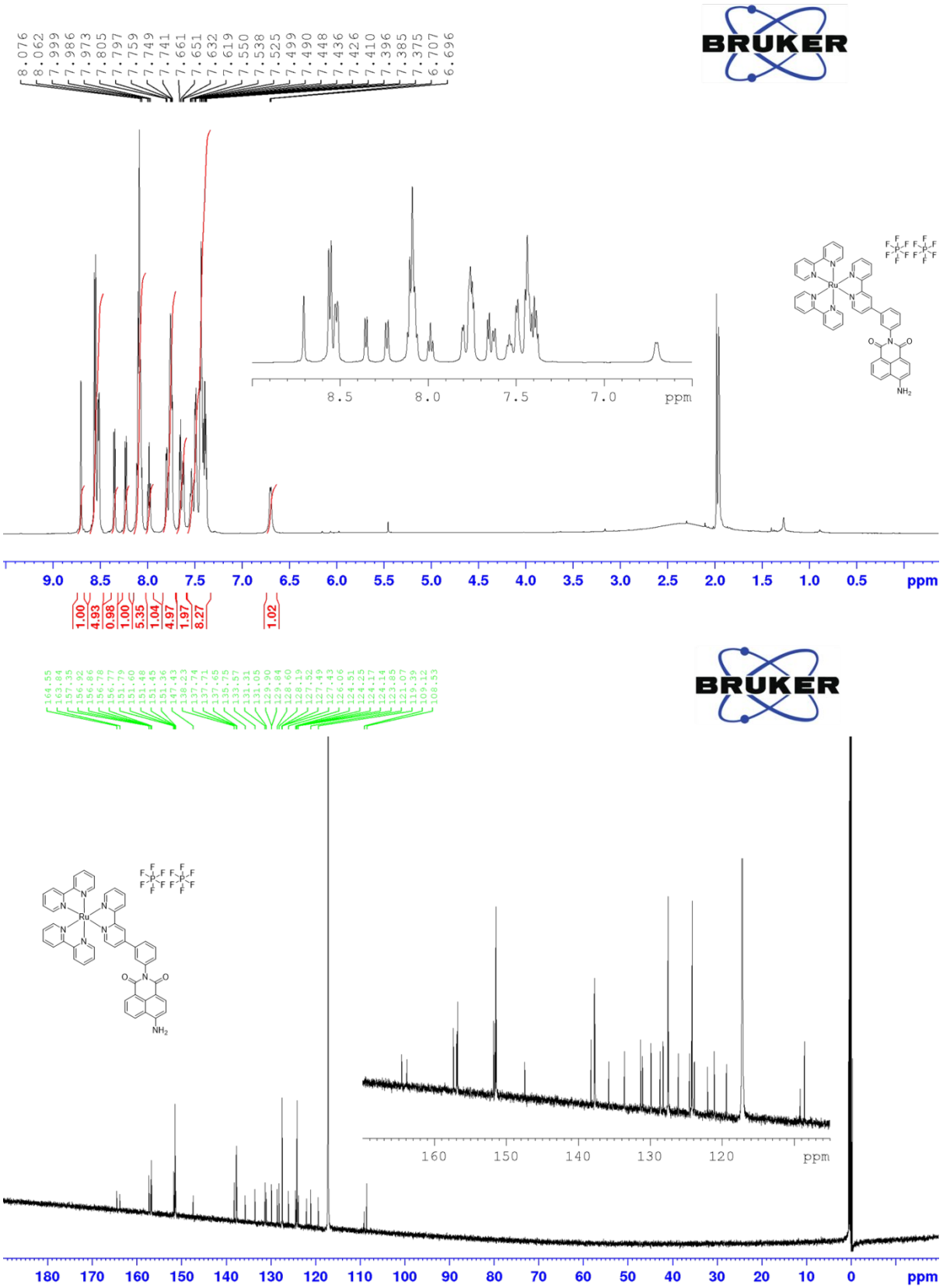

Figure S8: ^{1}H NMR (CD_3CN, 500 MHz) and ^{13}C NMR (CD_3CN, 125 MHz) spectra of **4**.

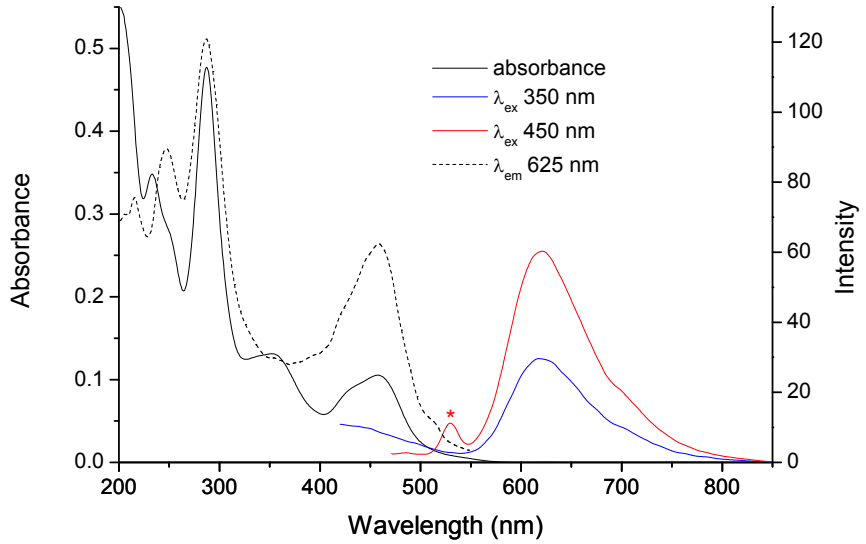

Figure S9: UV/Visible, excitation and emission spectra of **3** (6.5 μM) in 10 mM phosphate buffer, at pH 7. The water Raman band is denoted by *

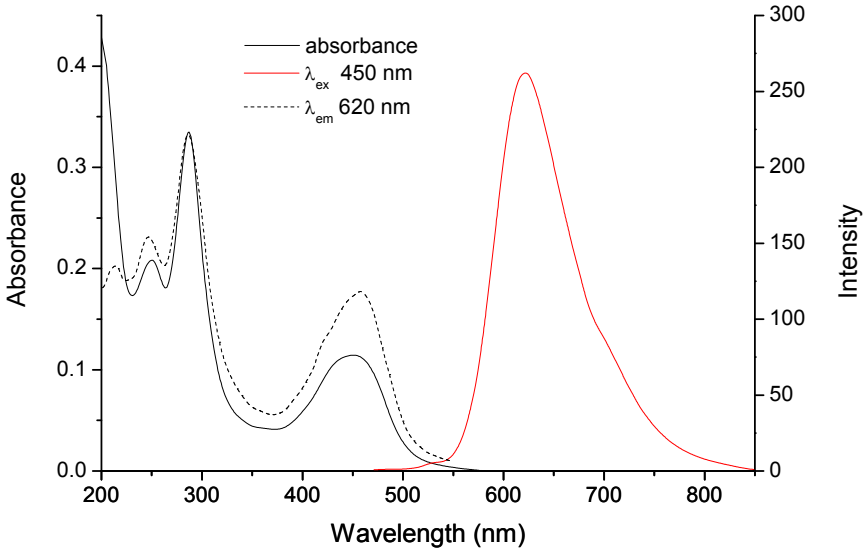

Figure S10: UV/Visible, excitation and emission spectra of **4** (6.5 μM) in 10 mM phosphate buffer, at pH 7.

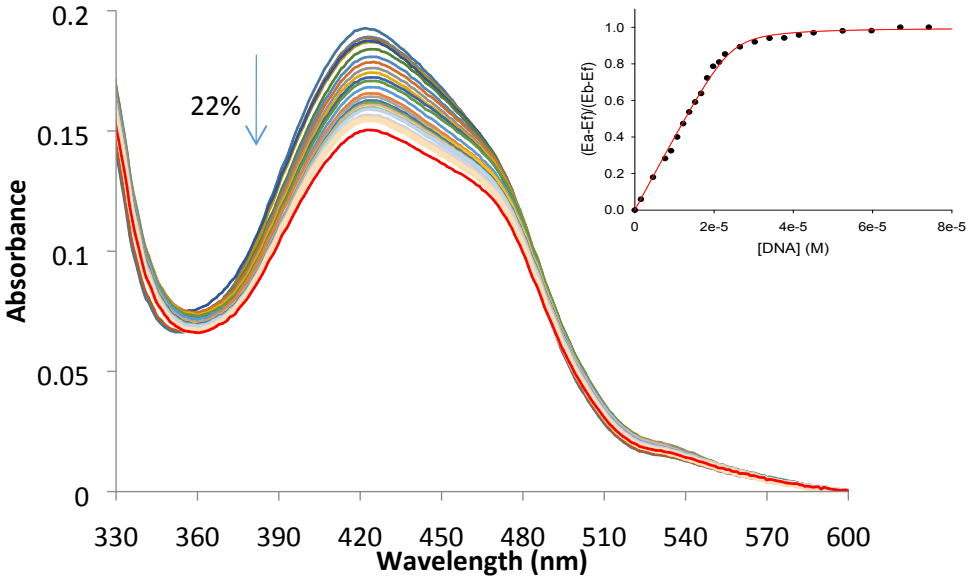

Figure S11: Changes in the UV/Visible spectrum of **2** (8 μM) with increasing additions of stDNA (0-210μM) in 10mM phosphate buffer, pH 7.4). Inset: Plot of $(\varepsilon_a-\varepsilon_f)/\varepsilon_b-\varepsilon_f)$ vs. [DNA](M^{-1}, P) using data with a P/D between 0-10 and the best fit of the data (---) using the Bard Eqn.

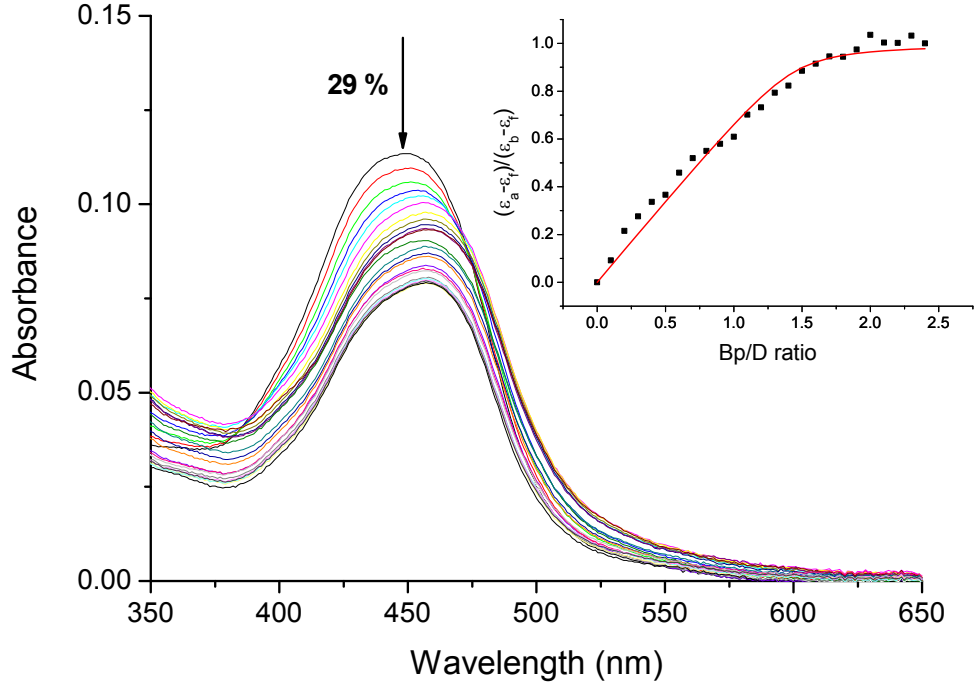

Figure S12: Changes in the UV/Visible spectrum of **4** (6.5 μM) upon addition of st-DNA (0 – 15.6 μM base pairs), both in 10 mM phosphate buffer, at pH 7. Inset: Plot of $(\varepsilon_a-\varepsilon_f)/(\varepsilon_b-\varepsilon_f)$ vs. equivalents of DNA and the corresponding non-linear fit.

(a)

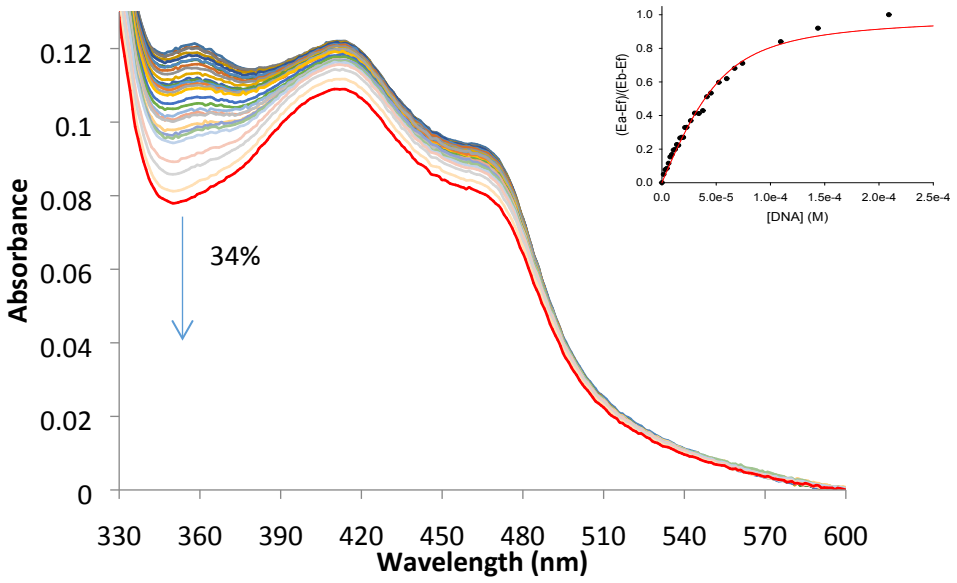

(b)

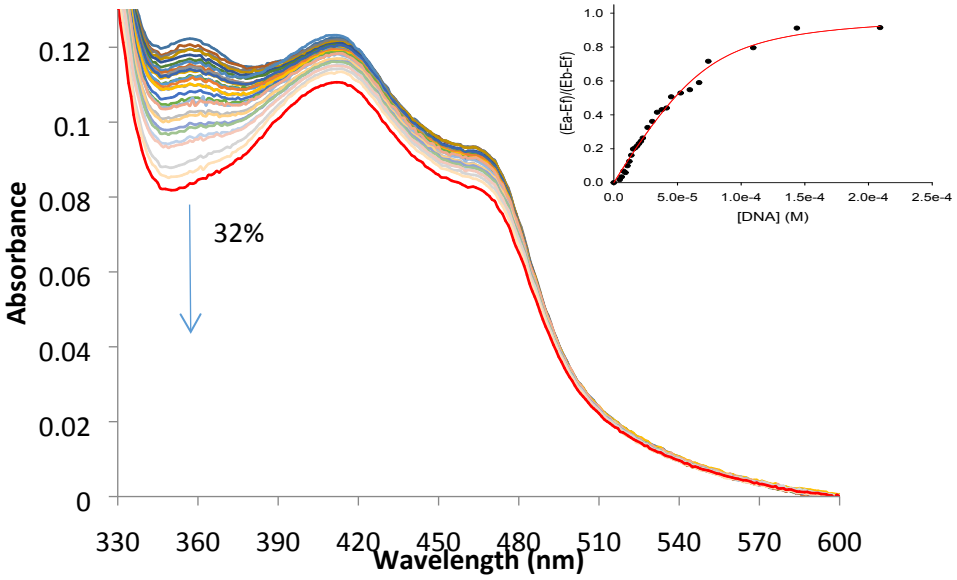

Figure S13: Changes in the UV/Visible spectrum of **1** (8 µM) with increasing concentration of stDNA (0-210 µM) at **(a)** 50 mM and **(b)**100 mM NaCl concentration. **Insets:** Plots of $(\varepsilon_a-\varepsilon_f)/\varepsilon_b-\varepsilon_f)$ vs. [DNA](M^{-1}, P) using data with a P/D between 0-12 and the best fit of the data (---) using the Bard Eqn.

(a)

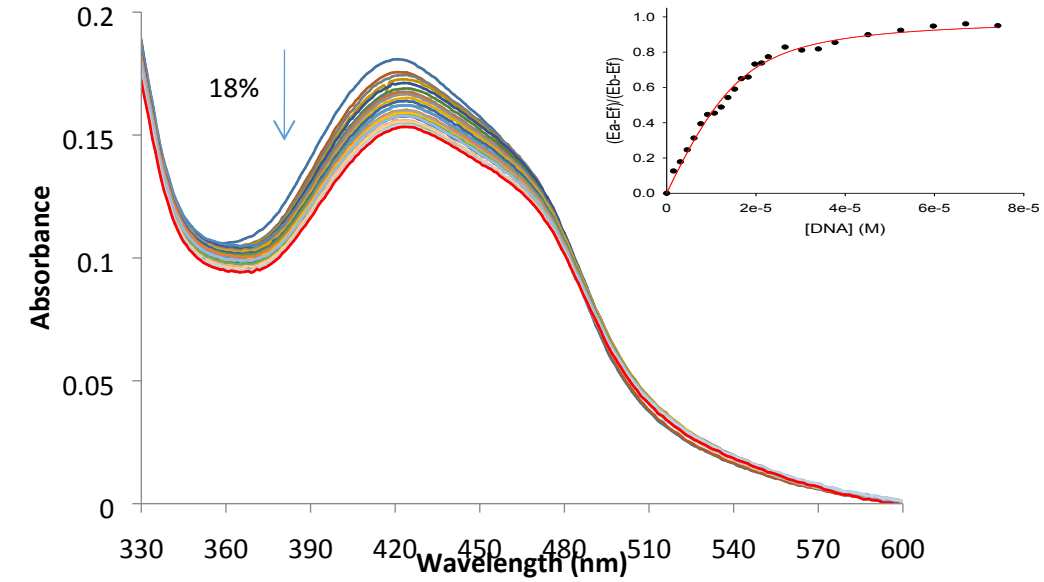

(b)

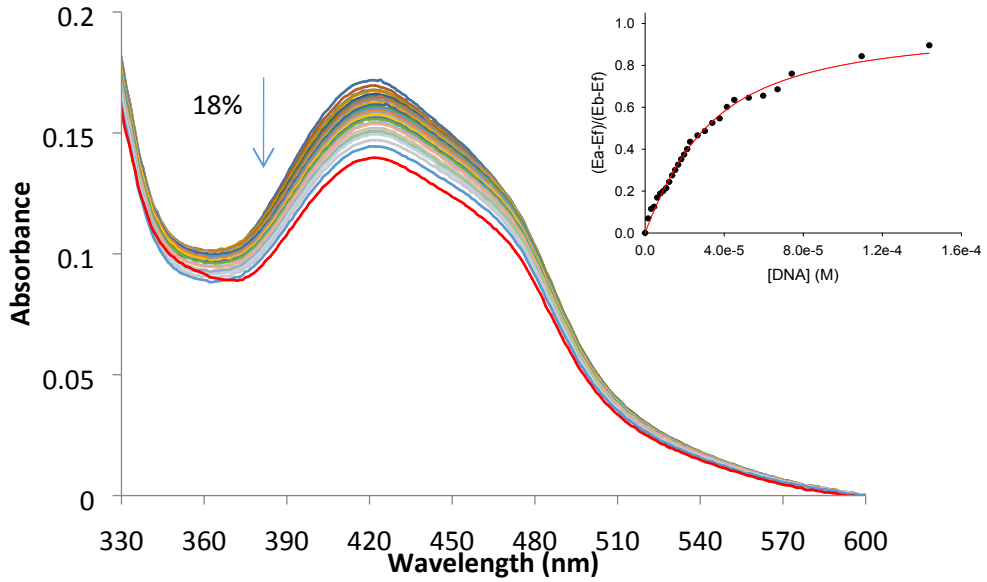

Figure S14: Changes in the UV/Visible spectrum of **2** (8 µM) with increasing concentration of stDNA (0-210 µM) at **(a)** 50 mM and **(b)**100 mM NaCl concentration. **Insets:** Plots of $(\varepsilon_a-\varepsilon_f)/\varepsilon_b-\varepsilon_f)$ vs. [DNA](M^{-1}, P) using data with a P/D between 0-12 and the best fit of the data (---) using the Bard Eqn.

(a)

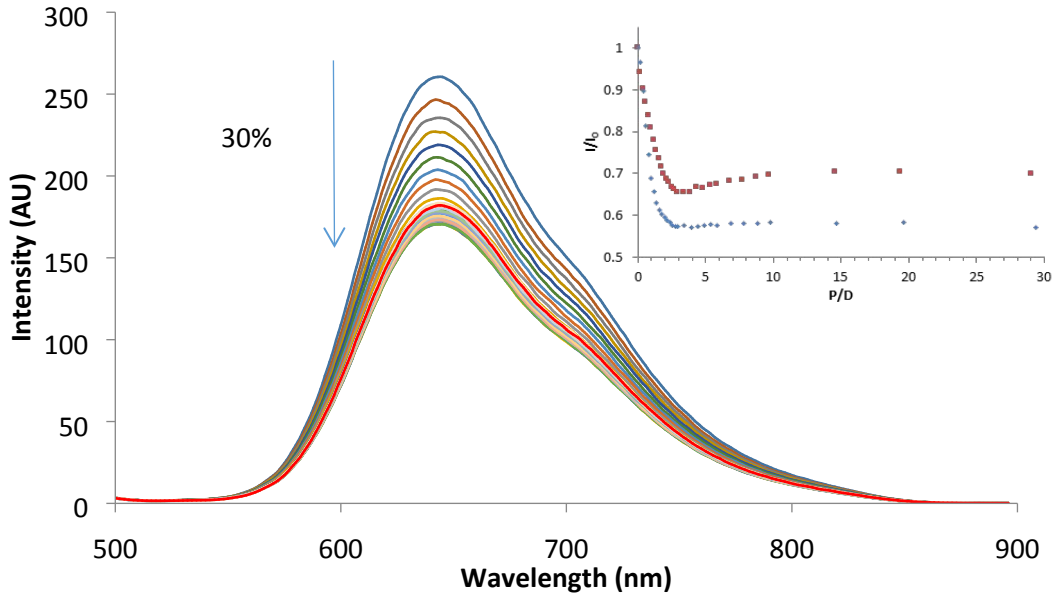

(b)

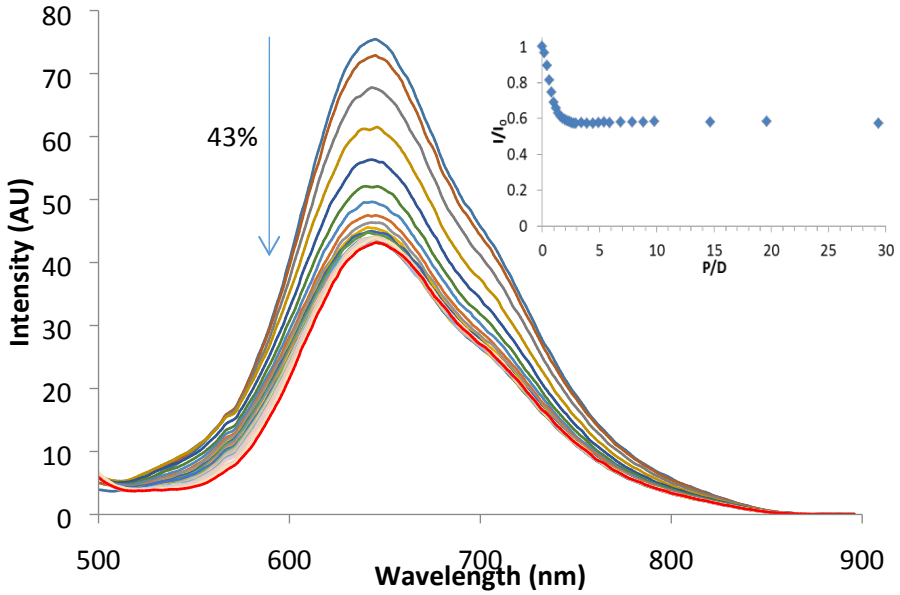

Figure S15: (a) Changes in the fluorescence emission spectrum of **1** (8 µM) (λ_{ex} = 415 nm) with increasing concentration of stDNA (0-210 µM). **Inset:** Relative changes in the emission intensity of **1** (■) and **2** (♦)(λ_{ex} = 415 nm) upon addition of stDNA in 10 mM phosphate buffer, at pH 7.4. **(b)** Changes in the emission spectrum of **2** (8 µM) (λ_{ex} 425 nm) with increasing concentration of stDNA (0-210 µM). **Inset:** Plot of the change in integrated MLCT emission intensity as a function of P/D ratio.

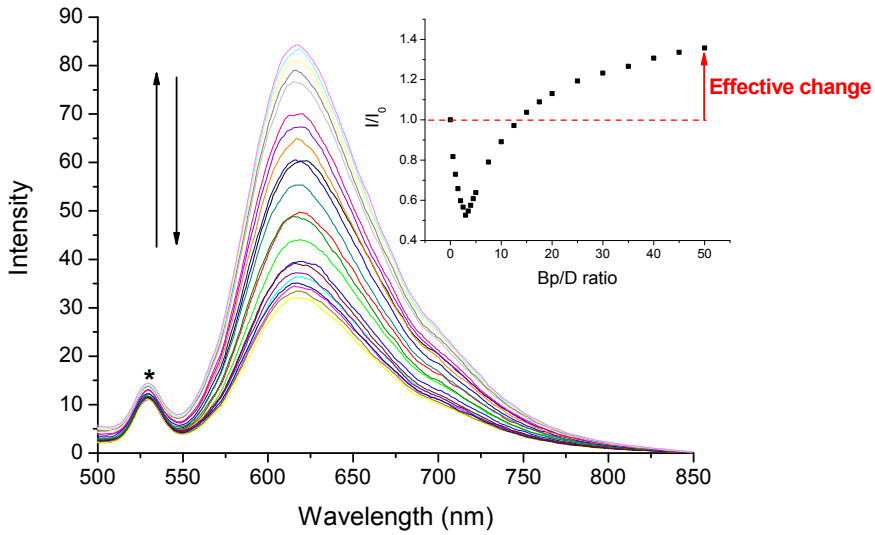

Figure S16: Changes in the emission spectrum of **3** (6.9 μM) (λ_{ex} 450 nm) upon addition of st-DNA (0 – 345 μM base pairs) in 10 mM phosphate buffer, at pH 7. The water Raman band is denoted by *. **Inset:** Plot of the change in integrated MLCT emission intensity as a function of Bp/D ratio.

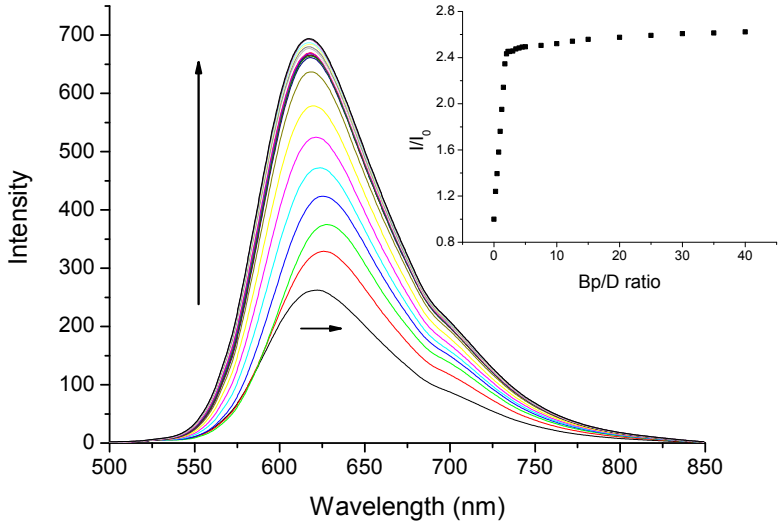

Figure S17: Changes in the emission spectrum of **4** (6.9 μM) (λ_{ex} 450 nm) upon addition of st-DNA (0 – 345 μM base pairs) in 10 mM phosphate buffer, at pH 7. The water Raman band is denoted by *. **Inset:** Plot of the change in integrated MLCT emission intensity as a function of Bp/D ratio.

(a)

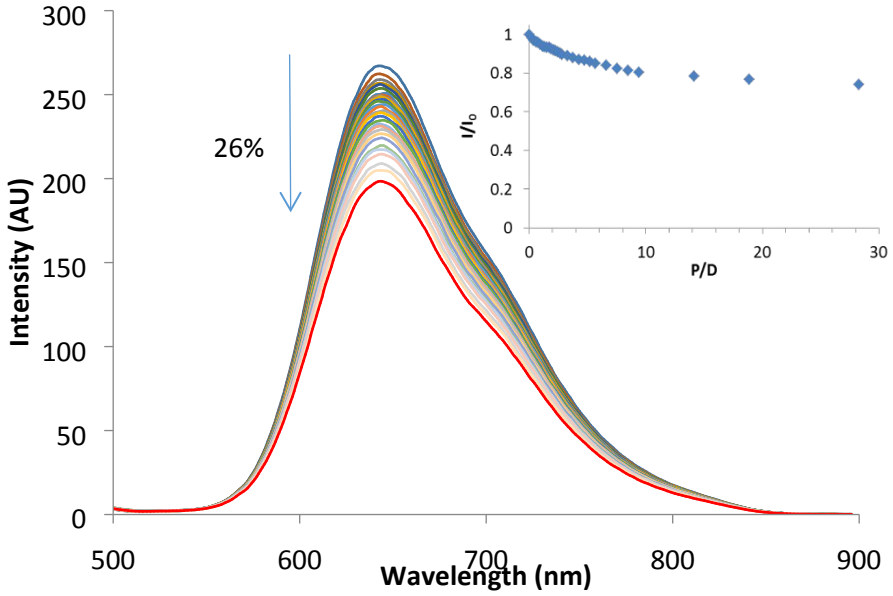

(b)

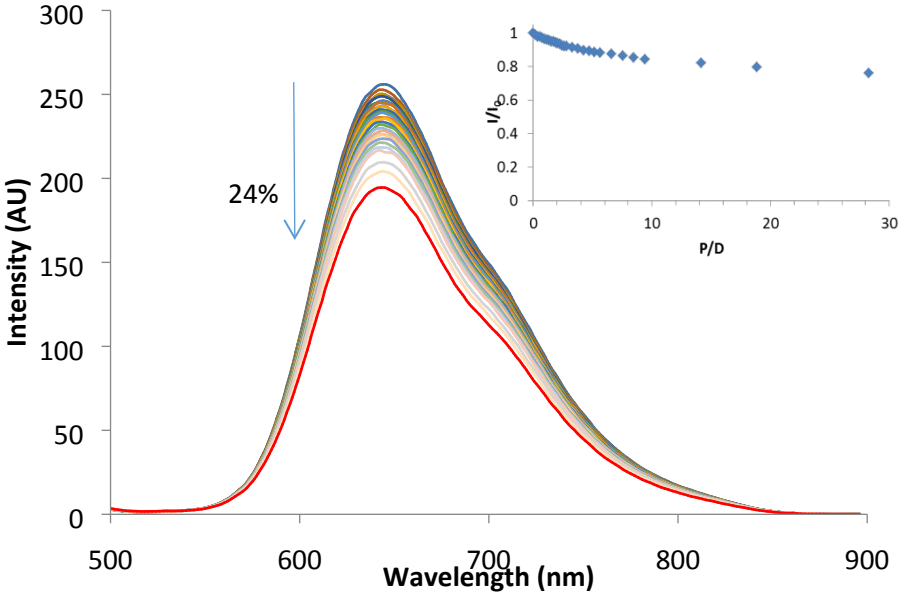

Figure S18: Changes in the fluorescence emission spectrum of **1** (8 μM) (λ_{ex} = 415 nm) with increasing concentration of stDNA (0-210 μM) at **(a)** 50 mM and **(b)**100 mM NaCl concentration. **Insets:** Plots of the change in integrated MLCT emission intensity as a function of P/D ratio.

(a)

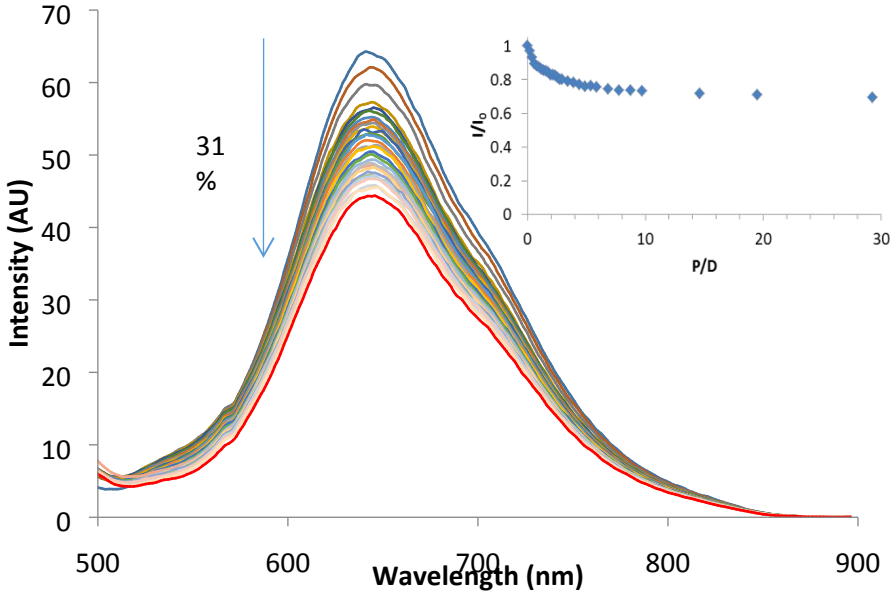

(b)

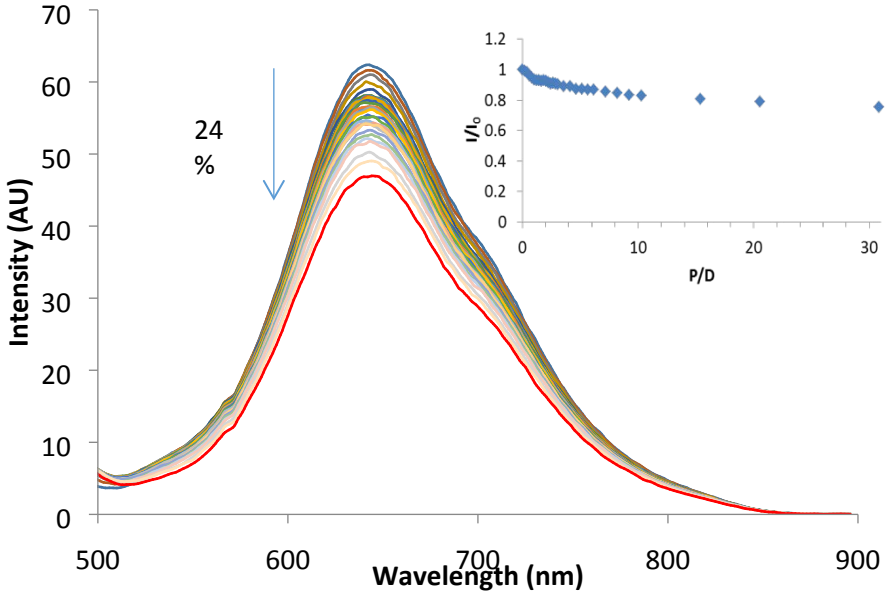

Figure S19: Changes in the fluorescence emission spectrum of **2** (8 μM) (λ_{ex} = 425 nm) with increasing concentration of stDNA (0-210 μM) at **(a)** 50 mM and **(b)**100 mM NaCl concentration. **Insets:** Plots of the change in integrated MLCT emission intensity as a function of P/D ratio.

Table S1: DNA binding parameters from fits to absorbance data at varying NaCl concentrations.

Complex	Binding constant K_b (M^{-1})	Binding site size n (base pairs)	R^2
1 + stDNA	1.3×10^6 (± 0.1)	1.3 (± 0.03)	0.99
1 + stDNA (50mM NaCl)	7.4×10^5 (± 0.9)	3.1 (± 0.03)	0.99
1 + stDNA (100mM NaCl)	4.3×10^5 (± 1.8)	4.45 (± 0.3)	0.99
2 + stDNA	5.8×10^6 (± 1.2)	1.50 (± 0.03)	0.99
2 + stDNA (50mM NaCl)	5.2×10^5 (± 0.9)	0.97 (± 0.07)	0.99
2 + stDNA (100mM NaCl)	1.2×10^5 (± 0.3)	1.3 (± 0.2)	0.99

(a)

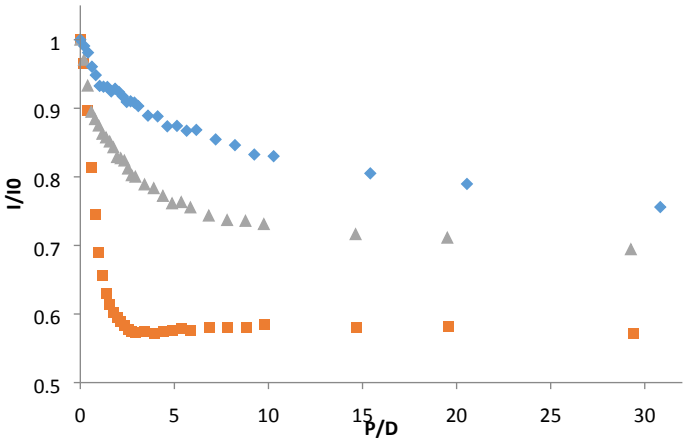

(b)

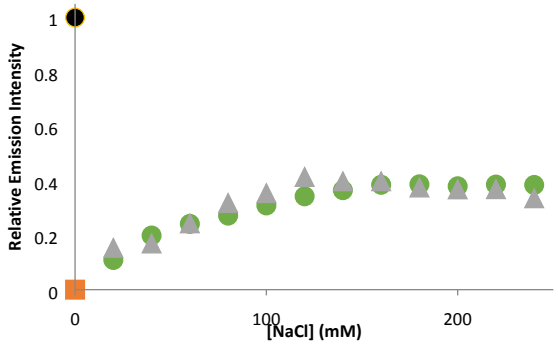

Figure S20: (a) Relative changes in the integrated emission intensity of **2** (8 µM) (λ_{ex} = 425 nm) with increasing concentration of st-DNA (0 – 210 µM), in 10 mM phosphate buffer (■), 10 mM phosphate buffer + 50 mM NaCl (▲) and 10 mM phosphate buffer + 100 mM NaCl (♦). (b) Fluorescence emission NaCl back titration profiles of **1** and **2** (λ_{ex} = 415 nm). Emission of unbound complex (●), fully bound complex (■) and bound **1**(▲) and **2** (●) in the presence of increasing concentration of NaCl.

(a)

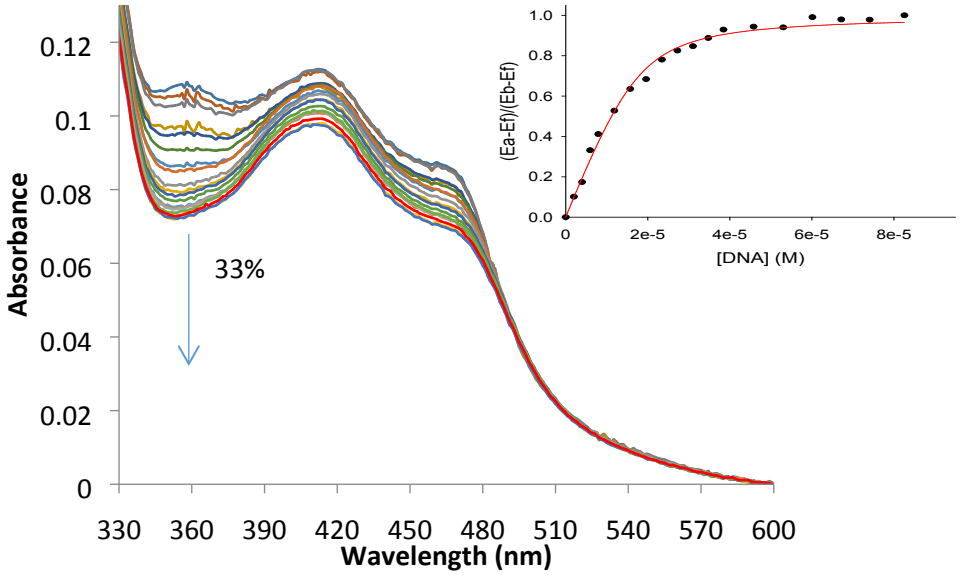

(b)

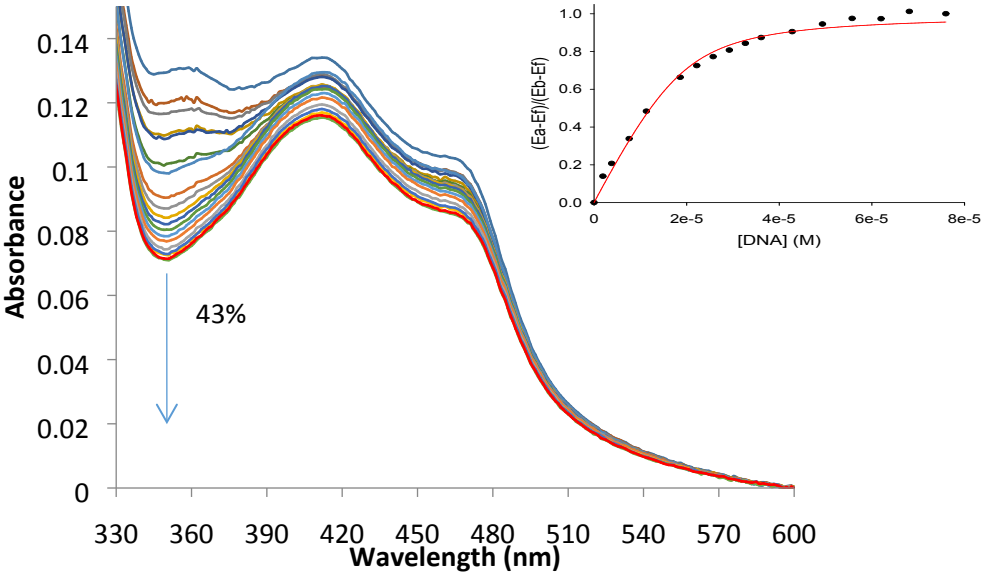

Figure S21: Changes in the UV/Visible spectrum of **1** (7.5 µM) with increasing concentration of **(a)** $[poly(dAdT)]_2$ (0-83µM) and **(b)** $[poly(dGdC)]_2$ (0-76µM) at pH 7.4. **Insets:** Plots of $(\varepsilon_a-\varepsilon_f)/\varepsilon_b-\varepsilon_f)$ vs. [DNA](M^{-1}, P) using data with a P/D between 0-12 and the best fit of the data (---) using the Bard Eqn.

(a)

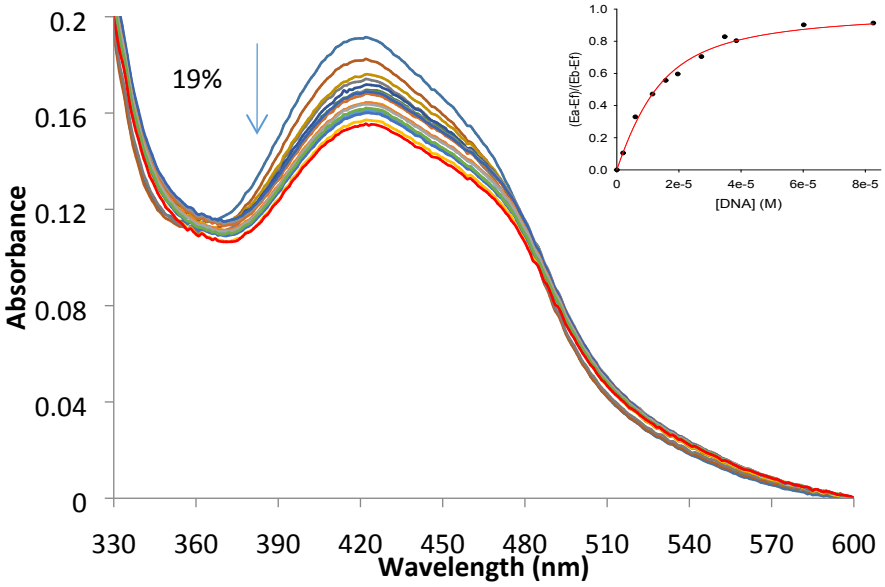

(b)

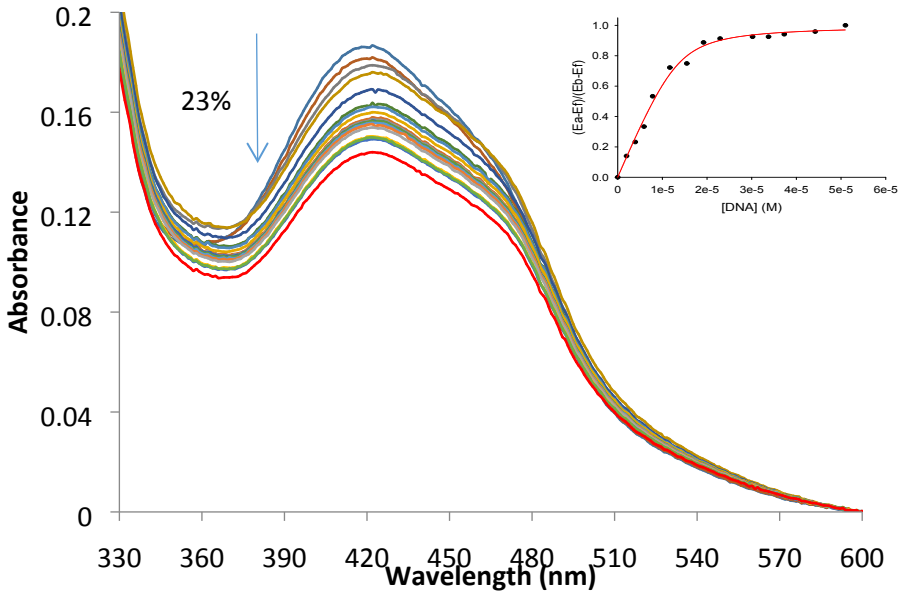

Figure S22: Changes in the UV/Visible spectrum of **2** (7.5 μM) with increasing concentration of **(a)** $[poly(dAdT)]_2$ (0-83 μM) and **(b)** $[poly(dGdC)]_2$ (0-78 μM) at pH 7.4. **Insets:** Plots of $(\varepsilon_a-\varepsilon_f)/\varepsilon_b-\varepsilon_f)$ vs. [DNA](M^{-1}, P) using data with a P/D between 0-12 and the best fit of the data (---) using the Bard Eqn.

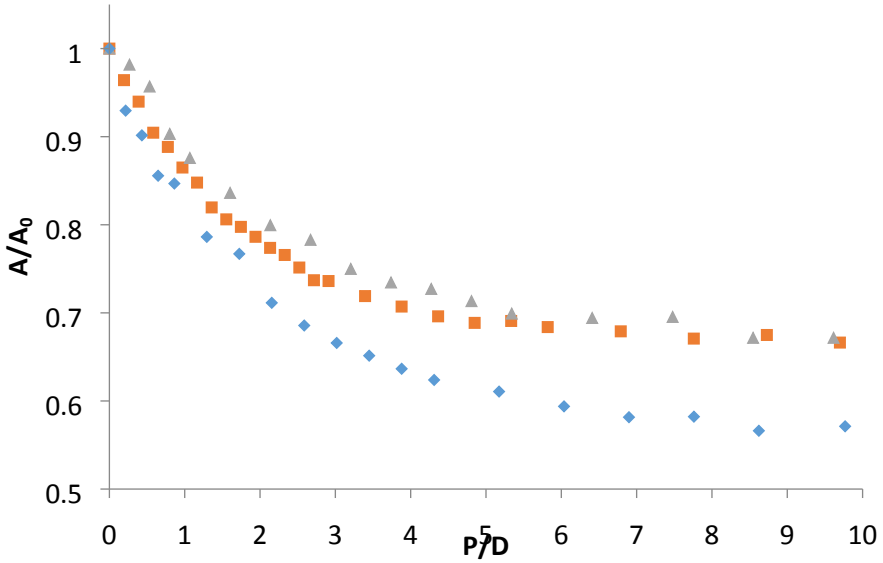

Figure S23: Changes in naphthalimide absorption at 358 nm of **1** (8 μM) in 10 mM phosphate buffer, at pH 7.4 upon addition of stDNA(■),[poly(dAdT)]$_2$ (▲) and [poly(dGdC)]$_2$ (◆).

Table S2: DNA binding parameters from fits to absorbance data in the presence of [poly(dAdT)]$_2$ and [poly(dGdC)]$_2$

Complex	λ(Naph) Hypo-chroism	λ(MLCT) Hypo-chroism	Binding constant K_b (M^{-1})	Binding site size *n* (base pairs)	R^2
1 + stDNA	37%	6%	1.3×10^6 (± 0.1)	1.3 (± 0.03)	0.99
1 + [Poly(dAdT)]$_2$	33%	12%	1.0×10^6 (± 0.2)	1.2 (± 0.1)	0.99
1 + [Poly(dGdC)]$_2$	43%	14%	8.5×10^5 (± 1.2)	1.1 (± 0.1)	0.99
2 + stDNA	----	22%	5.8×10^6 (± 1.2)	1.5 (± 0.03)	0.99
2 + [Poly(dAdT)]$_2$	----	19%	1.8×10^6 (± 0.7)	1.3 (± 0.03)	0.99
2 + [Poly(dGdC)]$_2$	----	23%	1.5×10^6 (± 0.4)	0.9 (± 0.06)	0.99

(a)

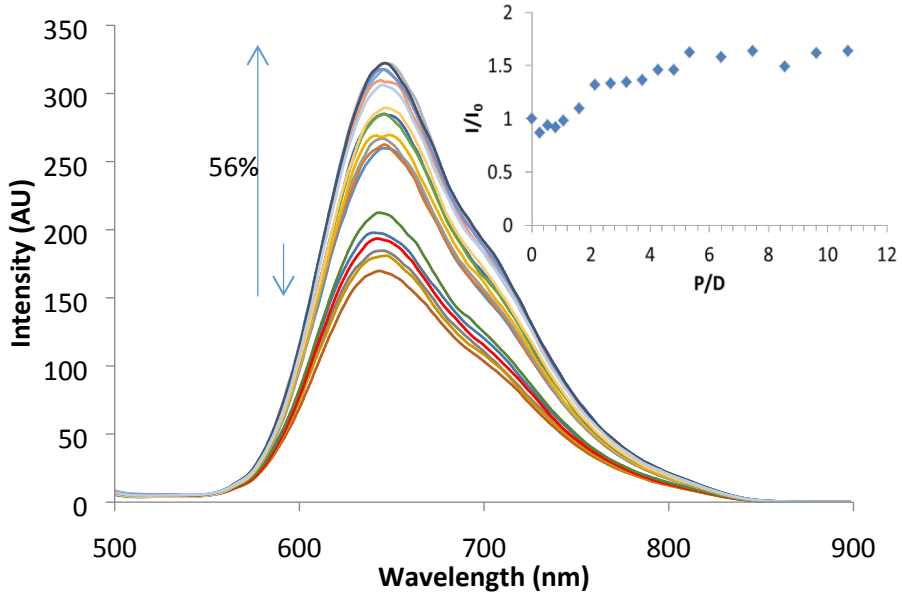

(b)

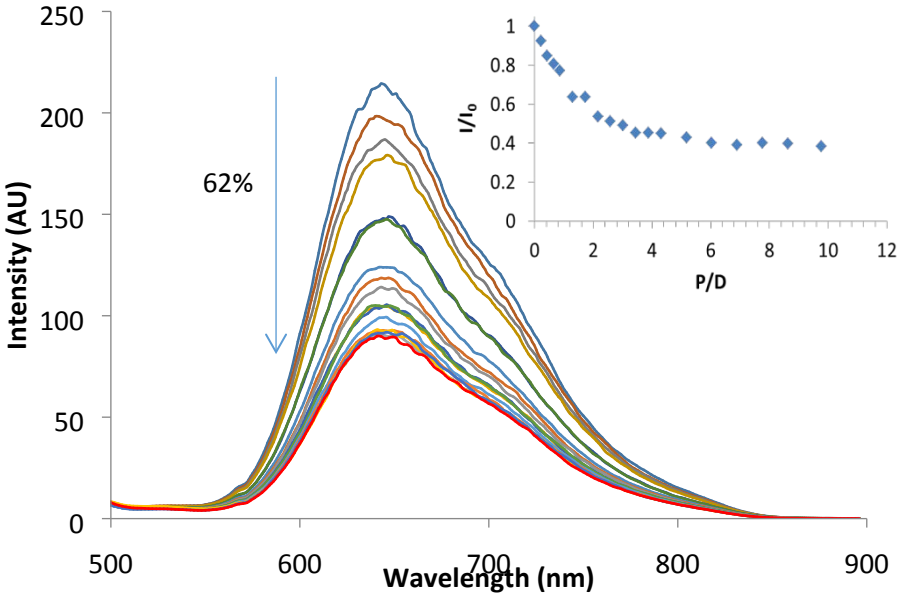

Figure S24: Changes in the fluorescence emission spectrum of **1** (8 μM) (λ_{ex} = 415 nm) with increasing concentration **(a)** $[poly(dAdT)]_2$ (0-83 μM) and **(b)** $[poly(dGdC)]_2$ (0-76 μM) at pH 7.4 **Insets:** Plots of the change in integrated MLCT emission intensity as a function of P/D ratio.

(a)

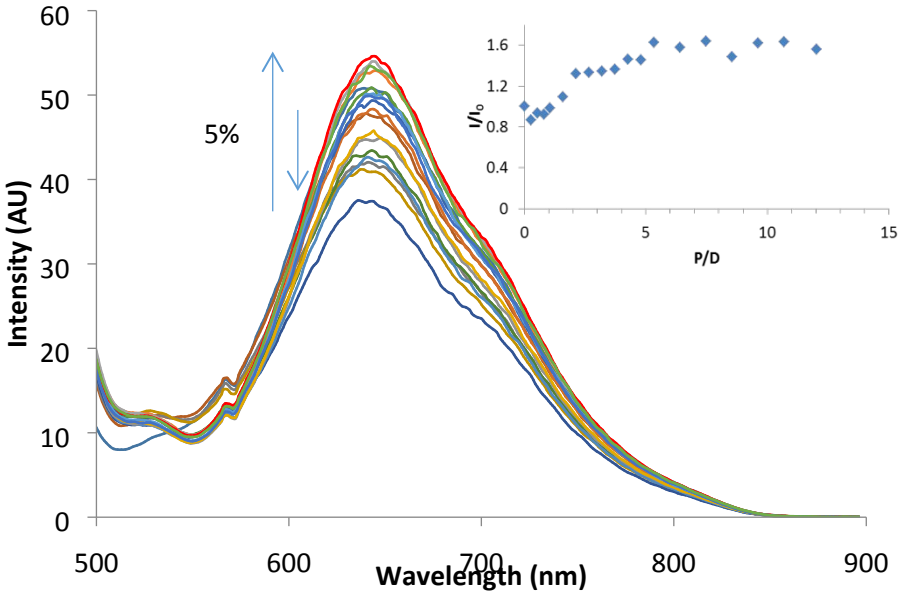

(b)

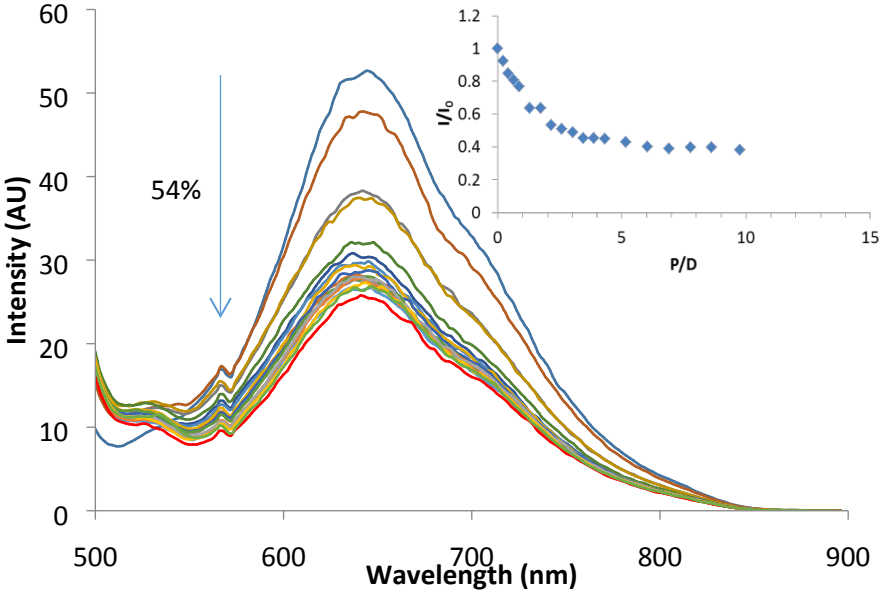

Figure S25: Changes in the fluorescence emission spectrum of **2** (8 µM) (λ_{ex} = 415 nm) with increasing concentration **(a)** $[poly(dAdT)]_2$ (0-83 µM) and **(b)** $[poly(dGdC)]_2$ (0-79 µM) at pH 7.4 **Insets:** Plots of the change in integrated MLCT emission intensity as a function of P/D ratio.

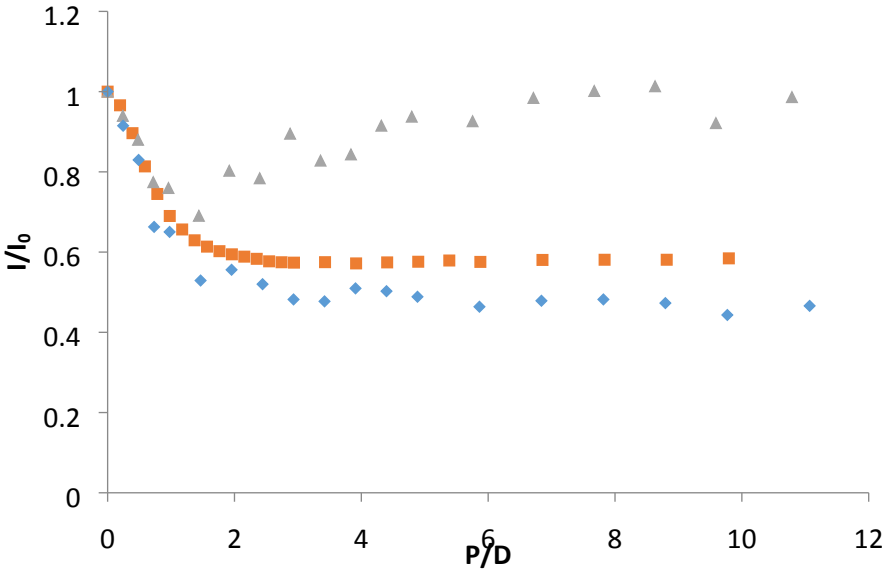

Figure S26: Relative changes in the integrated emission intensity of **2** (8 µM) (λ_{ex} 415 nm) with increasing concentration of stDNA(■), $[poly(dAdT)]_2$ (▲) and $[poly(dGdC)]_2$ (◆) in 10 mM phosphate buffer at pH 7.4.

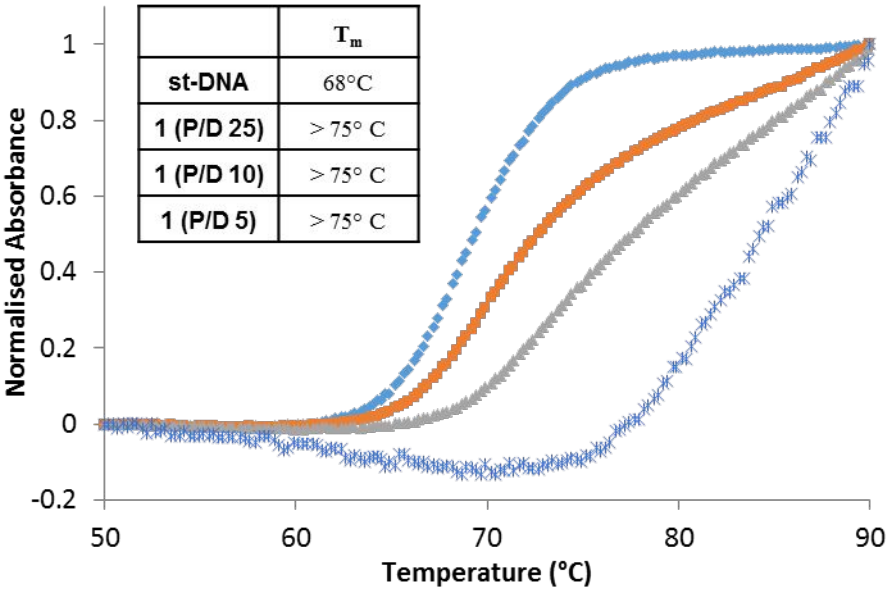

Figure S27: Thermal denaturation curves of stDNA (150 µM) in 10 mM phosphate buffer, pH 7.4, in the absence (♦) and presence of **1** at P/D = 25 (■) P/D = 10 (▲) and P/D = 5 (✳). **Inset:** The T_m values from first derivative plots of the melting curve.

(a)

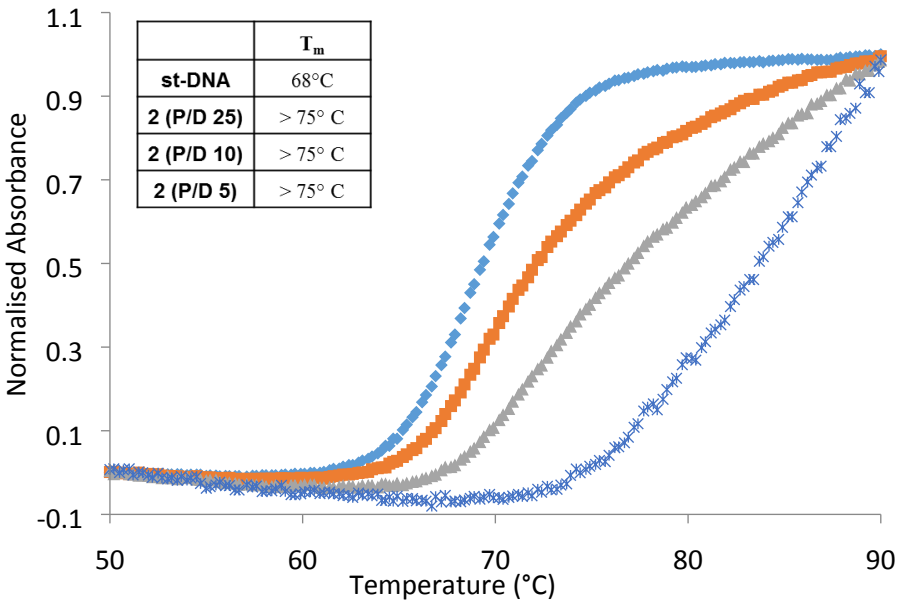

(b)

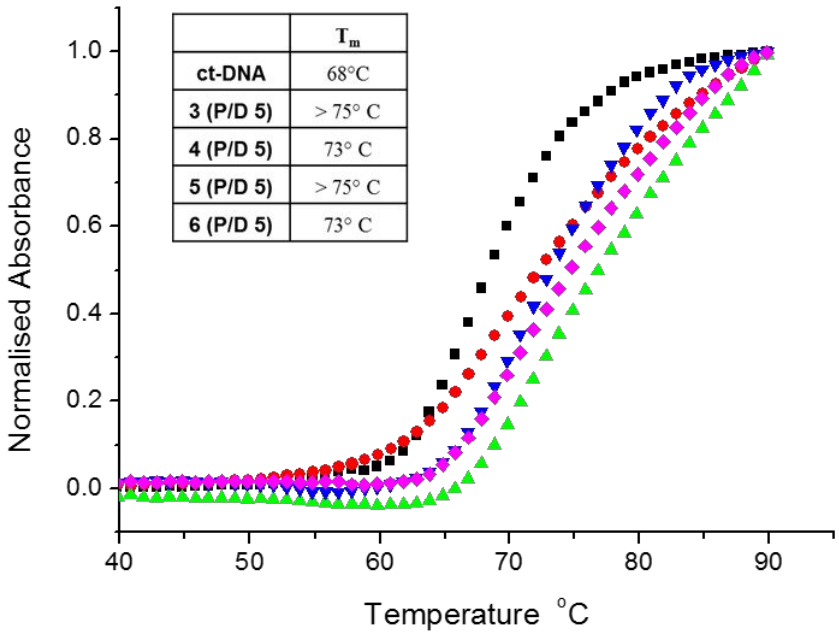

Figure S28: (a) Thermal denaturation curves of stDNA (150 µM) in 10 mM phosphate buffer, pH 7.4, in the absence (♦) and presence of **2** at P/D = 25 (■) P/D = 10 (▲) and P/D = 5 (✳). **(b)** Thermal denaturation curves of ct-DNA (150 µM) in 10 mM phosphate buffer, at pH 7, in the absence (■) and presence of **3** (▲), **4** (♦), **5** (●) and **6** (▼) at a Bp/D ratio of 5. **Insets:** The T_m values from first derivative plots of the melting curve.

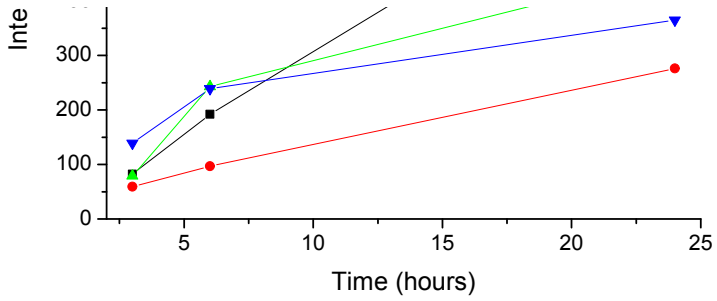

Figure S29: Observed fluorescence intensity from HeLa cells upon incubation with **3** (—●—), **4** (—▼—), **5** (—■—) and **6** (—▲—) all at a concentration of 12.5 μM.

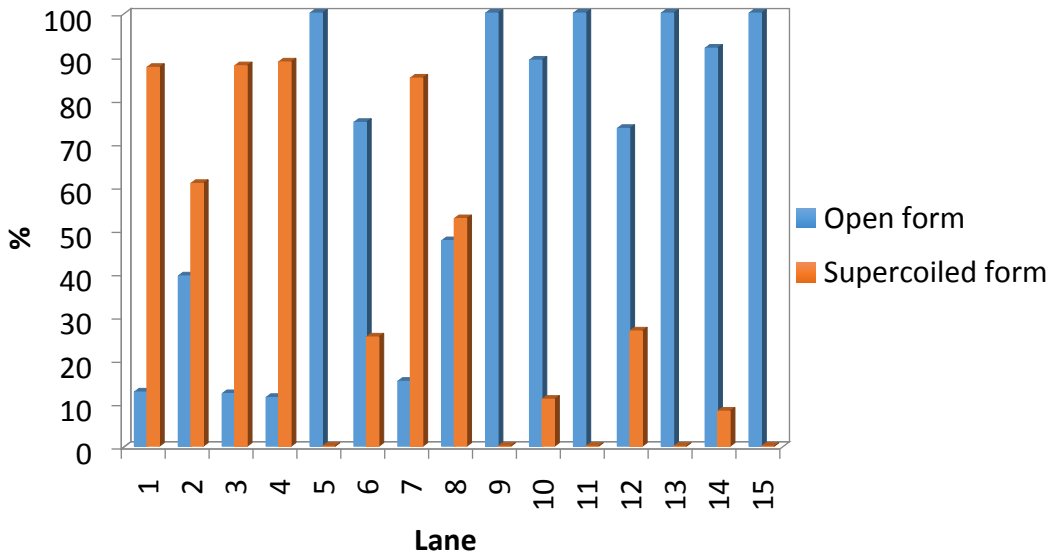

Figure S30: Relative percentages of supercoiled vs. open form pBR322 plasmid DNA from the photocleavage study of **1** – **4.**

Table S3: Summary of percentages of supercoiled vs. open form pBR322.

Lane	% Open	% Supercoiled	Lane	% Open	% Supercoiled
1	12.5	87.5	**9**	100	0
2	39.3	60.7	**10**	89.1	10.9
3	12.1	87.9	**11**	100	0
4	11.3	88.7	**12**	73.4	26.6
5	100	0	**13**	100	0
6	74.8	25.2	**14**	91.90	8.1
7	14.9	85.1	**15**	100	0
8	47.5	52.5			

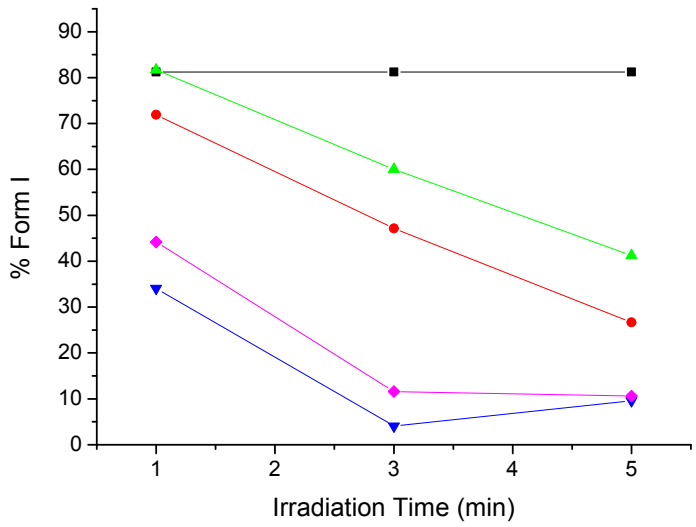

Figure S31: The % of form I pBR322 plasmid DNA remaining after irradiation in the absence (■) and presence of, **3** (▲),**4** (♦), **5** (●) and **6** (▼).

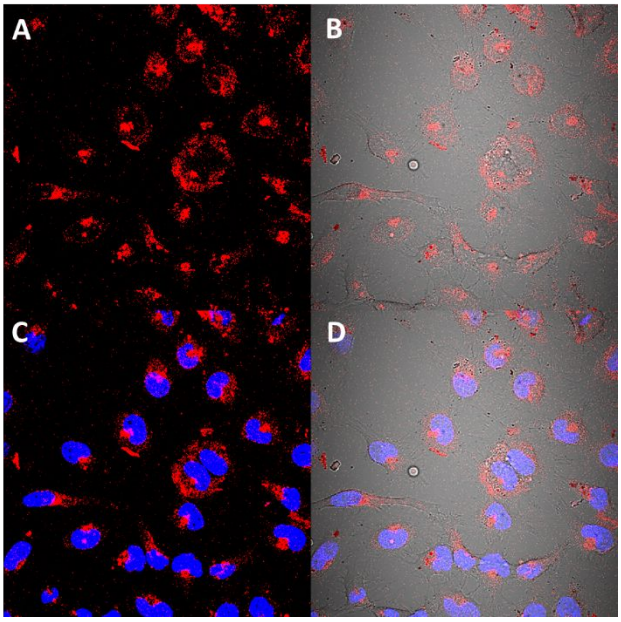

Figure S32: Confocal Laser Scanning Microscopy live cell images of **1** (50 µM) with HeLa cells. Shown is the image obtained with cells (A) stained with **1** (red), (B) overlay of **1** (red) and the bright field view, (C) overlay of **1** (red) and nuclear co-stain DAPI (blue) and (D) overlay of **1** (red), nuclear co-stain DAPI (blue) and the bright field view after 4 hrs of incubation.

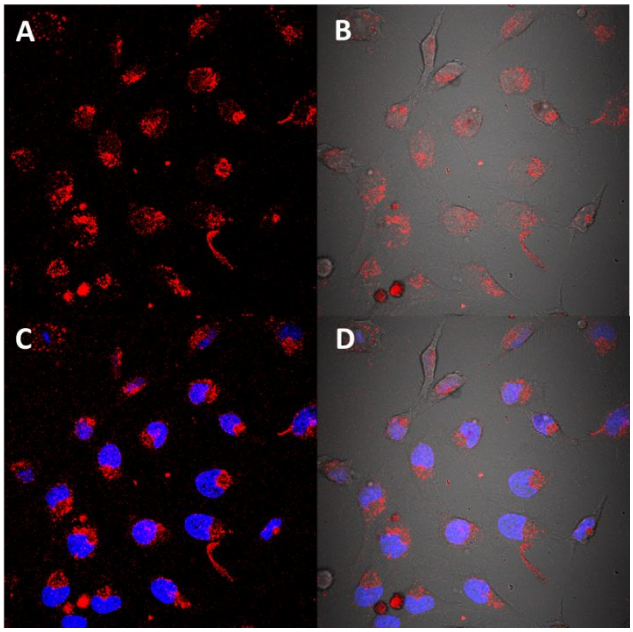

Figure S33: Confocal Laser Scanning Microscopy live cell images of **2** (50µM) with HeLa cells. Shown is the image obtained with cells (A) stained with **2** (red), (B) overlay of **2** (red) and the bright field view, (C) overlay of **2** (red) and nuclear co-stain DAPI (blue) and (D) overlay of **2** (red), nuclear co-stain DAPI (blue) and the bright field view after 4 hrs of incubation.

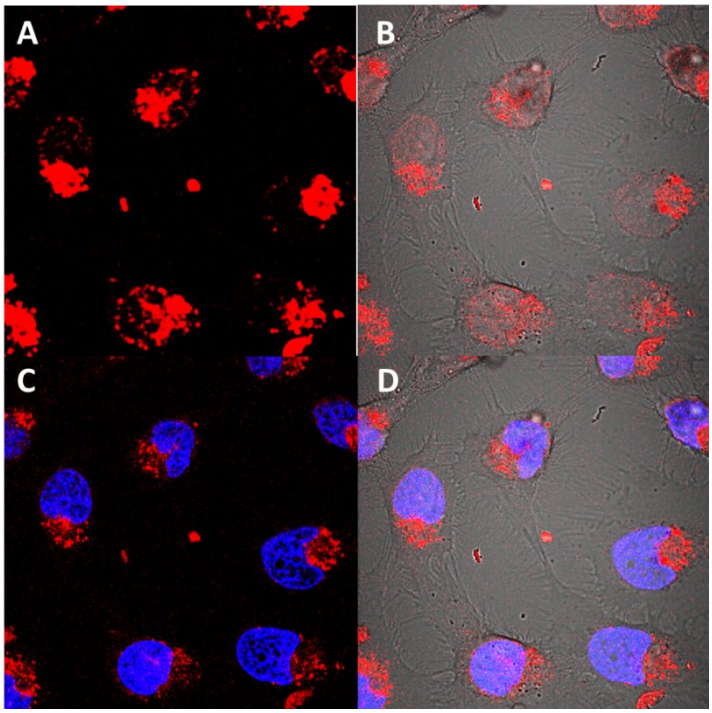

Figure S34: Confocal Laser Scanning Microscopy live cell images of **2** (50µM) with HeLa cells. Shown is the image obtained with cells (A) stained with **2** (red), (B) overlay of **2** (red) and the bright field view, (C) overlay of **2** (red) and nuclear co-stain DAPI (blue) and (D) overlay of **2** (red) , nuclear co-stain DAPI (blue) and the bright field view after 4 hrs of incubation.

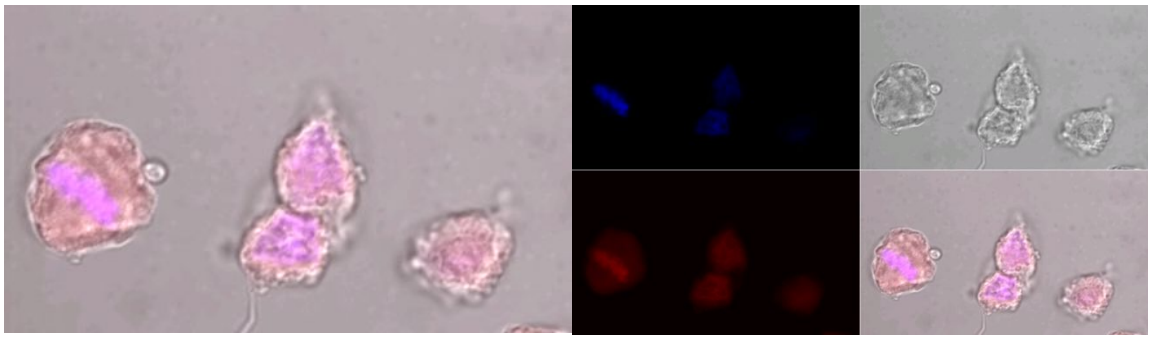

Figure S35: Confocal laser scanning microscopy image of **3** in HeLa cells. On the right is shown the image obtained of HOESCHT nuclear co-stain (blue), **3** (red), optical image of the cells (grey) and the overlay of these three. On the left is an enlarged version of the overlayed image.

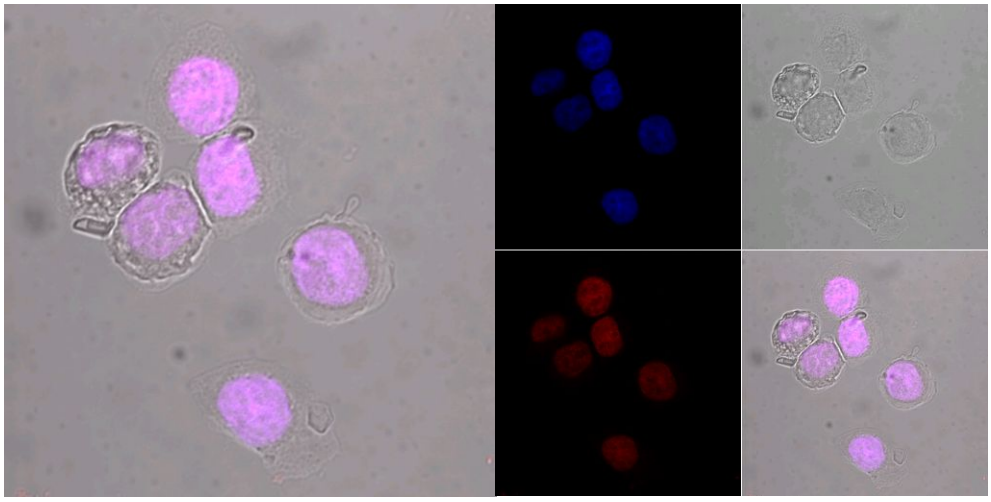

Figure S36: Confocal laser scanning microscopy image of **4** in HeLa cells. On the right shown the image obtained of HOESCHT nuclear co-stain (blue), **4** (red), optical image of the cells (grey) and the overlay of these three. On the left is an enlarged version of the overlaid image.

Table S4: Cell cycle analysis of K562 cells untreated or treated with 3 - 6 and irradiated with 8 J/cm^2.

	NT	NT+Irr	3	4	5	6
Sub-G_1	5.01 (±0.3)	5.75 (±0.1)	6.97 (±0.1)	12.7 (±0.2)	9.03 (±0.1)	16.3 (±0.1)
G_1	52.3 (±0.6)	50.8 (±0.1)	42.7 (±0.4)	25.7 (±0.3)	32.3 (±0.2)	22.8 (±0.3)
S	24.7 (±0.3)	27.8 (±0.3)	27.5 (±0.6)	21.3 (±0.1)	30.2 (±0.6)	27.6 (±0.1)
G_2/M	15.6 (±0.5)	15.1 (±0.3)	21.8 (±0.2)	38.2 (±0.8)	26.9 (±0.3)	29.9 (±0.5)

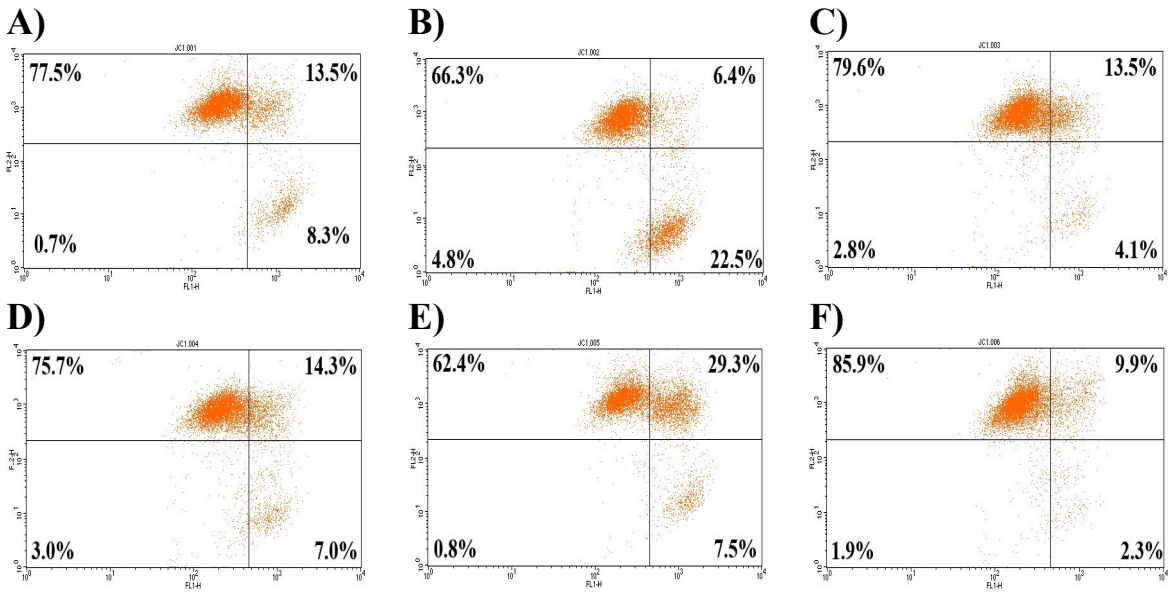

Figure S37: Flow cytometry plots of K562 cells treated with **3** - **6** in the dark. Cells were incubated with A) vehicle (RPMI medium), B) Etoposide (100 µM), C) **5** (10 µM), D) **6** (10 µM), E) **3** (10 µM) and F) **4** (10 µM) for 72 hours at 37 ºC in the presence of 5% CO_2 before they were analysed by flow cytometry as described in the text.

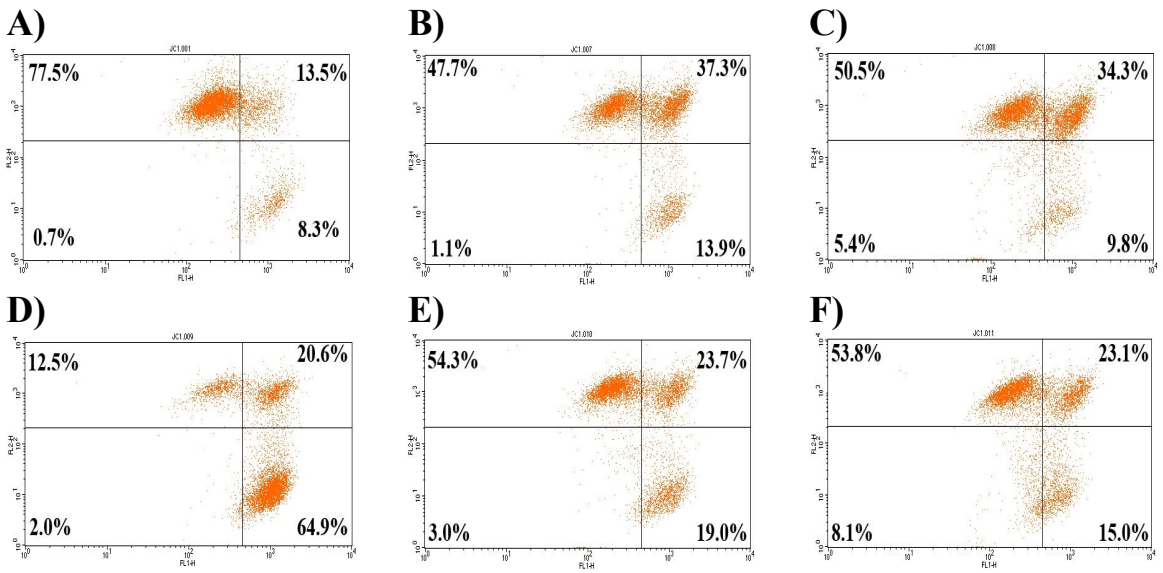

Figure S38: Flow cytometry plots of K562 cells treated with **3** - **6** and irradiated with 8 J/cm^2. Cells were incubated with A) vehicle (RPMI medium) in the dark, B) vehicle, C) **5** (10 µM), D) **6** (10 µM), E) **3** (10 µM) and F) **4** (10 µM) for 72 hours at 37 ºC in the presence of 5% CO_2 before they were irradiated with 8 J/cm^2 light dose. The cells were then incubated for 48 hours before being analysed by using flow cytometry as described in the text.

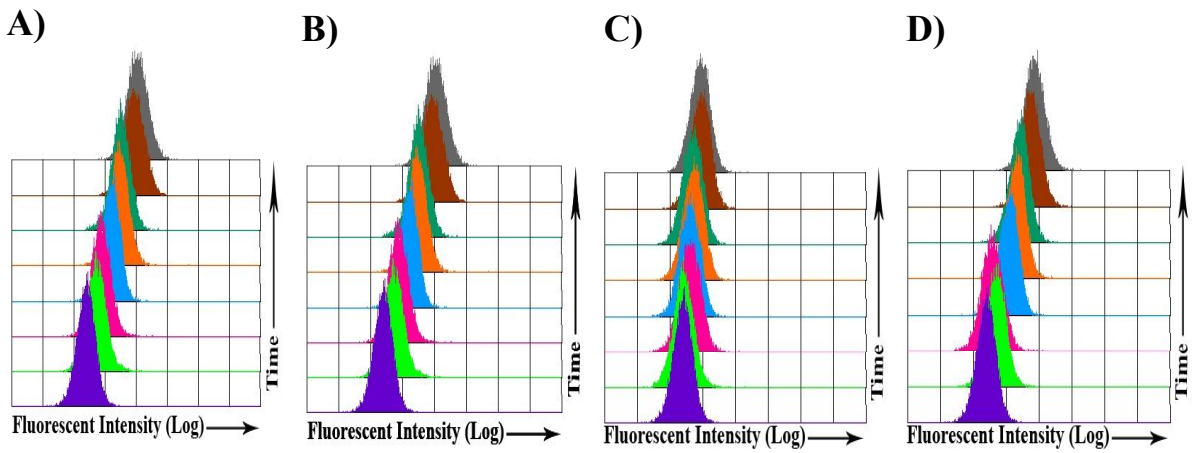

Figure S39: Plots of emitting fluorescence intensity from K562 cells. Cells were treated with A) **5** (1.0 µM), B) **6** (1.0 µM), C) **3** (1.0 µM) and D) **4** (1.0 µM) for 30 min. (■), 60 min. (■), 3 hours (■), 6 hours (■), 9 hours (■), 24 hours (■) and 48 hours (■). Untreated cells are shown as a solid purple peak. These plots are representative of three separate experiments.

References:

(1) Carter, M. T.; Rodriguez, M.; Bard, A. J. Voltammetric studies of the interaction of metal chelates with DNA. 2. Tris-chelated complexes of cobalt(III) and iron(II) with 1,10-phenanthroline and 2,2'-bipyridine. *Journal of the American Chemical Society* **1989**, *111*, 8901-8911.

(2) Sullivan, B. P.; Salmon, D. J.; Meyer, T. J. Mixed Phosphine 2,2'-Bipyridine Complexes of Ruthenium. *Inorg. Chem.* **1978**, *17*, 3334-3341.

(3) Rau, S.; Schäfer, B.; Grüßing, A.; Schebesta, S.; Lamm, K.; Vieth, J.; Görls, H.; Walther, D.; Rudolph, M.; Grummt, U. W.; Birkner, E. Efficient synthesis of ruthenium complexes of the type (R-bpy)2RuCl2 and [(R-bpy)2Ru(L-L)]Cl2 by microwave-activated reactions (R: H, Me, tert-But) (L-L: substituted bibenzimidazoles, bipyrimidine, and phenanthroline). *Inorganica Chimica Acta* **2004**, *357*, 4496-4503.

(4) Albers, M. O. S., Eric; Yates, Janet E. Dinuclear ruthenium(II) carboxylate complexes. . *Inorganic syntheses* **1989**, 249-258.

(5) Sheldrick, G. A short history of SHELX. *Acta Crystallographica Section A* **2008**, *64*, 112-122.

(6) Dolomanov, O. V.; Bourhis, L. J.; Gildea, R. J.; Howard, J. A. K.; Puschmann, H. OLEX2: a complete structure solution, refinement and analysis program. *Journal of Applied Crystallography* **2009**, *42*, 339-341.